



TALLINN UNIVERSITY OF TECHNOLOGY

SCHOOL OF ENGINEERING

Department of Materials and Environmental Technology

**TiO₂ ELECTRON TRANSPORTING LAYERS
SYNTHESIZED BY ALD AND USP METHODS FOR
Sb₂S₃ ABSORBER BASED SOLAR CELLS**

**ALD JA USP MEETODIL KASVATATUD TiO₂
ELEKTRONTRANSPORTKIHID Sb₂S₃ ABSORBERIL
PÕHINEVATELE PÄIKESEELEMENTIDELE**

MASTER THESIS

Student: Mudiaga Agbagidi

Student code: 213871KAYM

Supervisors: Tatjana Dedova, PhD,
Senior Research Scientist
Atanas Katerski, PhD,
Senior Research Scientist

Tallinn, 2024

AUTHOR'S DECLARATION

Hereby I declare, that I have written this thesis independently.

No academic degree has been applied for based on this material. All works, major viewpoints and data of the other authors used in this thesis have been referenced.

"11" January 2024

Author: Mudiaga Agbagidi



.....

Thesis is in accordance with terms and requirements

"....." January 2024

Supervisor: Tatjana Dedova

/signature/

"....." January 2024

Supervisor: Atanas Katerski

/signature/

Accepted for defence

"..11....." January 2024 .

Chairman of theses defense commission:

/name and signature/

Non-exclusive License for Publication and Reproduction of Graduation Thesis¹

I, Mudiaga Agbagidi hereby

1. grant Tallinn University of Technology (TalTech) a non-exclusive license for my thesis TiO₂ electron transporting layers synthesized by ALD and USP methods for Sb₂S₃ absorber based solar cells,

2.

(title of the graduation thesis)

supervised by Dr. Tatjana Dedova and Dr. Atanas Katerski,

(Supervisor's name)

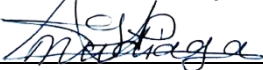
2.1 reproduced for the purposes of preservation and electronic publication, incl. to be entered in the digital collection of TalTech library until expiry of the term of copyright;

2.2 published via the web of TalTech, incl. to be entered in the digital collection of TalTech library until expiry of the term of copyright.

2.3 I am aware that the author also retains the rights specified in clause 1 of this license.

3. I confirm that granting the non-exclusive license does not infringe third persons' intellectual property rights, the rights arising from the Personal Data Protection Act or rights arising from other legislation.

11.01.2024 (date)



¹ The non-exclusive licence is not valid during the validity of access restriction indicated in the student's application for restriction on access to the graduation thesis that has been signed by the school's dean, except in case of the university's right to reproduce the thesis for preservation purposes only. If a graduation thesis is based on the joint creative activity of two or more persons and the co-author(s) has/have not granted, by the set deadline, the student defending his/her graduation thesis consent to reproduce and publish the graduation thesis in compliance with clauses 1.1 and 1.2 of the non-exclusive licence, the non-exclusive licence shall not be valid for the period.

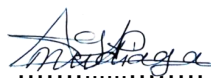
Thesis tasks and time schedule:

| No | Task description | Deadline |
|----|--|------------|
| 1. | Literature overview | 15.02.2023 |
| 2. | Deposition of TiO ₂ thin films on glass and as solar cell component by ALD and USP methods | 15.04.2023 |
| 3. | Study of optical and structural properties of TiO ₂ films on glass | 20.06.2023 |
| 4. | Recording the I-V curves of SC with glass/FTO/ALD TiO ₂ /Sb ₂ S ₃ /HTM/Au and glass/FTO/USP TiO ₂ /Sb ₂ S ₃ /HTM/Au structures | 25.10.2023 |
| 5. | Literature overview and processing of the obtained data | 05.11.2023 |
| 6. | Submission of the initial draft to the supervisors | 24.12.2023 |

Language: English

Deadline for submission of thesis: 09.01.2024

Student: Mudiaga Agbagidi



"..11....."January.....2024

/signature/

Supervisor: Tatjana Dedova

"..11....." January.....2024

/signature/

Supervisor: Atanas Katerski

"..11....."January.....2024

/signature/

Head of study programme: Sergei Bereznev

"..11....." January..... 2024

/signature/

Terms of thesis closed defence and/or thesis restricted access conditions to be formulated on the reverse side.

THESIS TASK

Student: Mudiaga Agbagidi, 213871KAYM

Study programm, KAYM09, Materials and Processes for Sustainable Energetics

Supervisor(s):

Tatjana Dedova, PhD, Senior Research Scientist, Department of Materials and Environmental Technology, Thin Film Energy Materials Lab (tatjana.dedova@taltech.ee)

Atanas Katerski, PhD, Senior Research Scientist, Department of Materials and Environmental Technology, Thin Film Energy Materials Lab (atanas.katerski@taltech.ee)

Thesis topic:

TiO₂ electron transporting layers synthesized by ALD and USP methods for Sb₂S₃ absorber based solar cells,

ALD ja USP meetodil kasvatatud TiO₂ elektrontransportkihid Sb₂S₃ absorberil põhinevatele päikeseelementidele

Thesis main objectives:

1. To synthesize and characterize TiO₂ films as electron transport layers (ETL) by ALD and USP methods as main components of Sb₂S₃ based solar cells
2. To evaluate the performance of complete SC devices based on ALD and USP electron transport layers by I-V, Kelvin probe and PYS measurements
3. To determine the best performing ETL TiO₂ layer synthesis method and conditions.

CONTENTS

| | |
|---|----|
| PREFACE | 7 |
| LIST OF ABBREVIATIONS AND SYMBOLS | 9 |
| INTRODUCTION..... | 10 |
| 1. LITERATURE REVIEW | 12 |
| 1.1 Building Integrated Photovoltaics. Semitransparent solar cells..... | 12 |
| 1.2 Sb ₂ S ₃ based Semitransparent Solar Cells..... | 12 |
| 1.3 Electron transport material..... | 14 |
| 1.4 TiO ₂ thin films properties | 15 |
| 1.5 Thin films deposition methods..... | 16 |
| 1.5.1 Atomic Layer Deposition (ALD) | 16 |
| 1.5.2 Ultrasonic Spray Pyrolysis (USP)..... | 18 |
| 2. CHARACTERIZATION METHODS | 20 |
| 2.1 Thin Films Characterization Techniques | 20 |
| 2.1.1 Scanning Electron Microscope | 20 |
| 2.1.2 UV-Vis Spectroscopy | 21 |
| 2.1.3 X-ray Diffraction..... | 22 |
| 2.2 Solar cells characterization techniques..... | 24 |
| 2.2.1 Current voltage characteristics..... | 24 |
| 2.2.2 Kelvin Probe Spectroscopy (KPS) | 25 |
| 3. RESULTS AND DISCUSSION | 29 |
| 3.1 Experimental | 29 |
| 3.1.1 Thin Film Deposition | 29 |
| 3.1.2 Thin film and SC Characterization | 30 |
| 3.2 Results..... | 31 |
| 3.2.1 Structural and Optical Properties of ALD and USP TiO ₂ Layers | 31 |
| 3.2.2 SC Output Parameters..... | 34 |
| 3.2.3 Electronic properties and band alignment of SC components in SC structure..... | 36 |
| SUMMARY..... | 39 |
| KOKKUVÕTE | 41 |
| LIST OF REFERENCES..... | 43 |

PREFACE

The topic for this Thesis was suggested by the Head of the Thin Film Energy Materials Laboratory, Lead Researcher Ilona Oja Acik. This work was performed in the frame of current projects: Estonian Research Council (project PRG627), the Archimedes SA (Estonian Centre of Excellence Project TK141 (TAR16016EK), the European Commission's H2020 programme under the ERA Chair (grant agreement No 952509). The research was conducted using the NAMUR+ core facility funded by the Estonian Research Council (TT 13). The practical research was conducted at the Laboratory of Thin Film Energy Materials at TalTech. Senior Researcher Tatjana Dedova and Senior Researcher Atanas Katerski provided guidance throughout experimental work and thesis writing.

The objective of this thesis was to prepare and study the electron transport layer properties and suitability, TiO_2 , as a core component for a semi-transparent solar cell with configuration of glass/FTO/ TiO_2 / Sb_2S_3 /HTM/Au. We compared two different techniques of TiO_2 preparation, ALD and USP and study the obtained solar cell performance. The research was divided into sub sections:

1. Deposition of TiO_2 layers on glass substrates by ALD (different thicknesses of TiO_2 were produced) and USP methods
2. Characterization of the TiO_2 layers
3. Preparation and study the performance of a semi-transparent solar cell with configuration of glass/FTO/ TiO_2 / Sb_2S_3 /HTM/Au incorporating of ALD and USP TiO_2 ETL layers

I express my gratitude to my supervisors, Senior Researcher Tatjana Dedova and Senior researcher Atanas Katerski for their guidance and support during experimental work and thesis writing process. I also express my gratitude to Dr. Marin Rusu for electrical measurements of solar cells and Dr. Olga Volobujeva for SEM images. I would like to share my special thanks to the head of the laboratory, Tenure Professor Ilona Oja Acik, for opening me the opportunity to conduct this research in the Thin Films Energy Lab. I am sincerely grateful to my family, who kindly supported me on this journey.

Key words: solar cell, electron transport layer, TiO_2 , ALD, USP, I-V, PYS

LIST OF ABBREVIATIONS AND SYMBOLS

ALD-Atomic Layer Deposition

BIPV - Building Integrated Photovoltaic

E_g - Band gap energy

ETL – Electron Transport Layer

ETM – Electron Transport Material

EQE - External quantum efficiency

GPC - Growth rate per cycle

J_{sc} - Short circuit current

HTL – Hole Transport Layer

I-V -Current voltage characteristics

KP - Kelvin Probe

PYS - Photon Yield Spectroscopy

PCE - Photoconversion efficiency

SC – Solar Cell

SEM - Scanning electron microscopy

TCO - Transparent conductive oxide

USP – Ultrasound Spray Pyrolysis

V_{oc} - Open circuit voltage

XRD - X-ray diffraction

INTRODUCTION

Solar cells have been one of the major devices for producing clean energy. Every year 173,000 TW (terawatts) of energy from the sun reaches the earth in form of solar radiation. This is about 10,000 times the global consumption of energy and this shows there is great potentials for solar energy to meet our growing energy demands [1]–[3]. In 2021, solar cells accounted for 5% of energy production globally. Solar cells work on the principle of photovoltaic effect discovered by Edmond Becquerel in 1839[4]–[6]. The photovoltaic effect is a phenomenon that occurs when sunlight strikes a semiconductor material and electrical current is produced[4], [7]. From the discovery of the photovoltaic effect, scientists and engineers have studied this phenomenon to develop better ways to harvest solar energy and improve photovoltaic material technology.

Solar cells over the years have tremendously improved from the first crystalline silicon (c-Si) cells with 4.5% PCE [8] to current efficiency of single-junction monocrystalline silicon of 26.7 ± 0.5 %. In recent times the building integrated photovoltaic (BIPV), tandem solar cells and for indoor applications desired the use of thin films solar cells with bifaciality and semitransparent properties [9], [10]. Thin film solar cells which have been reported efficient have been the monofacial and opaque forms, this was because of the use of metallic contact for both the substrate and superstrate configuration as make for the solar cell. The limitation of this form of solar cells is that they are not semitransparent enough for use as BIPV windows [11]. Therefore, their capacity in term of performance in diffused incident light is limited [11], [12].

It is significant to note that the transparency of crystals making up the thin film solar cells are important properties necessary for the expression of efficiency in functioning as a thin layer solar cell complementing the essence of a silicon solar cell. In a quest to cover for this limitation the $Sb_2(S, Se)_3$ for use as a photovoltaic material has shown potential in the absorption coefficient, bandgap control and its sustainability [13], [14]. The antimony chalcogenide [$Sb_2(S, Se)_3$] with this positive alternative prospect has recorded a 10.7% PCE recently in the literature [15]. Typical solar cells comprise of few components which are found between the electrode of the circuit system, they include; the electron transport layer (ETL), the hole transporting layer (HTL), the absorption layer usually (chalcogenide) [16]. The transport and the extraction of photogenerated electrons from the electron transport layer and the absorber interface to the electrode of the solar cells is done by the ETL [16]. Therefore, there is need for carefully select the material type for this layer meeting the conditions of thickness, structure, optical and electrical properties. The optimization of this component of the solar cell done theoretically and technologically improves it reproducibility efficiency and the efficacy of the photoconversion process, therefore providing a perfect alignment of the

interfacial energy levels and reducing the possibility of charges recombination [17]–[19]. In this work we study the solar cell with FTO/TiO₂/Sb₂S₃/P3HT/Au heterojunction present based on ETL TiO₂ layers, deposited by ultrasonic spray pyrolysis (USP), and atomic layer deposition (ALD), respectively. To understand the mechanism of FTO/TiO₂/Sb₂S₃/P3HT/Au heterojunctions, the Kelvin probe (KP) and PYS (Photon Yield Spectroscopy) measurements were performed.

Obtained TiO₂ layers were characterized by SEM, XRD, and UV-VIS techniques.

This work was initiated by Head of Laboratory (Prof. Ilona Oja Acik) and senior staff of a Thin Film Energy Materials Laboratory including Tenure Prof. Malle Krunk, Senior Research Scientist Atanas Katerski and a continuation of the study on semitransparent solar cells based on Sb₂S₃ absorber layers[20], [21].

The main hypothesis of the thesis is that TiO₂ material synthesized by ALD and spray pyrolysis methods are suitable ETL layers owing a good electronic configuration match with Sb₂S₃ absorber layer. In order to prove the hypothesis, the solar cell with FTO/TiO₂/Sb₂S₃/P3HT/Au heterojunction was prepared and analyzed, where TiO₂ is grown by ALD and USP methods. Specifically, this work accomplishes three main tasks:

1. To synthesize and characterize TiO₂ films as electron transport layers (ETL) by ALD and USP methods as main components of Sb₂S₃ based solar cells
2. To evaluate the performance of complete SC devices based on ALD and USP electron transport layers by I-V, Kelvin probe and PYS measurements
3. To determine the best performing ETL TiO₂ layer synthesis method and conditions.

This thesis consists of three main sections:

1. Literature review – this section provides an overview of the importance of semitransparent solar cell, advantage of Sb₂S₃ absorber based semitransparent solar cells, electron transport material functions and TiO₂ electron transparent material as an appropriate choice, applied in this work technologies for the deposition of TiO₂ ETM layers and description of characterization
2. Methods – this section presents description of the methods of TiO₂ as a main solar cell component and a whole solar cell structure.
3. Results – This section includes the results, analyses and conclusions of the experimental study, and suggests future research directions.

1. LITERATURE REVIEW

1.1 Building Integrated Photovoltaics. Semitransparent solar cells

Building integrated photovoltaics has been one of the most promising applications of photovoltaics. This is different from building-attached PV where PV modules are attached to the body or roof of building systems. Over the years, several applications of BIPV's have existed and are in development. These range from solar windows, glasses, roofs, facades and other building components. BIPV's serve five main purposes; reducing carbon footprint, renewable energy generation, building energy efficiency improvement, effective space utilization, and enhancing aesthetic appeal.

In the global scene and in the European Union (EU), there have been steady growth in the market for BIPV's, with an annual growth rate of 18.7% in 2019[22]. This is driven by many factors including greater support for research and development in BIPVs, funding, and policy initiatives. In the EU specifically, the Energy Performance of Building Directive (EPBD) 2010/31/EU[23] and the Energy Efficiency Directive 2012/27/EU[24] are the major drivers toward the growth of BIPVs as they can play a vital role in meeting the targets of Net-Zero energy buildings by 2030 through on-site renewable energy generation. Integrating BIPV's could also reduce operational carbon emissions of buildings by up to 50%[25].

In recent years, there have been significant developments in BIPV materials, incorporating a wide range of highly efficient thin film transparent/semi-transparent photovoltaic materials due to their lightweight, high level of flexibility compared to crystalline silicon, superior thermal properties, and overall cost advantages. Common second-generation PV materials such as a-Si, CdTe, CIGS, and CIS have been investigated and used in BIPV applications. Reports of CdTe and CIGSSe have been recorded to have 22.1 and 23.4 % power conversion efficiencies respectively [26], [27]. They are expensive and require the use of sophisticated vacuum-based deposition methods for their fabrication, especially inorganic thin films. Methods such as vacuum vaporation and magnetron sputtering have been reported used [27]. Due to the expenses involved in it fabrication, the toxic nature of the metals (Cd and Se) and their scarcity, the use of Sb_2Se_3 has become prominent [28], [29].

1.2 Sb_2S_3 based Semitransparent Solar Cells

The Sb_2S_3 material is an excellent material for the solar cell component due to its unique properties. Some of these properties include a high absorbance coefficient of $18 \times 10^3 \text{ cm}^{-1}$ at 450nm, a band gap of 1.7 eV, stability in air and water, abundance in nature and a sustainable-green material [30]. The synthesis of this material is possible with high

crystallinity at low temperature, this is because of the low melting point exhibited by the Sb_2S_3 . It also has a better electron collection efficiency, due to this diffusion length of 290-900nm. These properties are accountable for the materials excellence application as a solar cell component especially as an absorber layer.

A solar cell with the Sb_2S_3 material as a component to make up a device is similar in some ways to a dye-sensitized solar cell. This device includes also an electron transport layer, hole transport materials, photon absorption layer and a back contact (Fig. 1). When photons are incident on the material surface, electrons in the valence band of the Sb_2S_3 material absorbs this energy and gets excited. These excited electrons get transported into the TiO_2 layer [31]. Holes are then generated on the surface of the material and moves toward the p-type hole transport layer. These holes are then collected by the back contact of the solar cell. There exists an external connection between the photo-anode and the back contact of the cell. This connection leads to follow the electron rich photo-anode to the back contact through external load leading to the generation of electricity [32]. Commonly used electron transport material includes TiO_2 , ZnO , CdS , and SnO_2 [33]. Commonly used hole transport materials include copper thiocyanate (CuSCN), poly (3-hexylthiophene) (P3HT), spiro-OMeTAD, NiO_x , V_2O_5 , gel polymer electrolyte and liquid electrolyte. Finally, commonly used back contacts for solar cells include Au and Ag, including carbon which has recently been used both as the hole transport material and as a back contact in Sb_2S_3 solar cells [34]–[36]. So far the record efficiency for Sb_2S_3 solar cell is 7.5% and theoretically can be largely improved by developing a perfectly matching p-n junction partner materials, such as electron transport material [37].

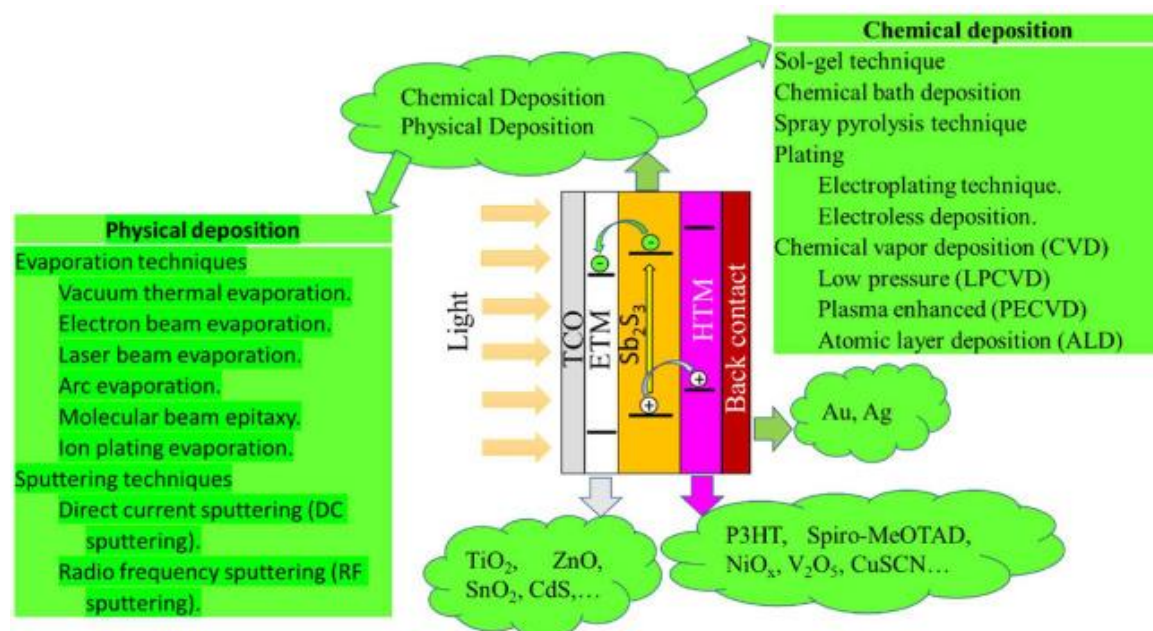


Figure 1. Schematic diagram of solid-state nanocrystalline Sb_2S_3 thin-film solar cells and the deposition methods; ETM, HTM refer the electron transport materials and hole transport materials, respectively [9].

As can be seen from the figure, various methods exist to obtain Sb_2S_3 material including physical and chemical ones. Compared to physical methods chemical methods, such as chemical bath deposition, hydrothermal growth, spray pyrolysis techniques are markedly cost-effective (no need for costly vacuum), easy to operate and control the product properties through the technology [20], [21]. In this work spray pyrolysis have been chosen as simple, proven, reliable method to produce high quality Sb_2S_3 thin film absorber layers.

1.3 Electron transport material

In solar cells the most significant component is the ETL which has garnered attention recently in scientific literature in a quest to advance and develop it [29]. The properties of this layer chiefly dictate the performance of the designed solar cell. This component functions in the extraction of electrons from the absorber and the transport of the electrons to the contact electrodes. The ETL can also function as an energy blockage for hole transport. Finally, the EL serves as a nucleation center for the cell (perovskite) which has significant effect on the optical property of the optoelectronic performance via affect the growth of crystals [38], [39]

In the selection of electron transport materials (ETMs) for the design of solar cells certain criteria must be met. These criteria include; the coverage of the electrode or absorber layer. This ensures the prevention of pinhole formation and shunting. The ETMs used must be both planar and mesoporous. This is to allow for high optical transmittance and high refractive index preventing optical losses. The ETMs must also align such that the conduction band minimum and both the CBM of the absorber for electron extraction and the work function of the electrode for ohmic contacting. Other criteria for ETMs are in its stability and fabrication conditions which should be kept in mild. For ETMs to function effectively there also must have great electron mobility for ease of electron transport.

In literature so far, CdS materials stands out as the most common and classical ETL material for the design of antimony chalcogenide solar cells [40], [41]. With a low band gap of 2.4 eV, CdS leads to current loses in solar cell; this is caused by parasitic absorption of electrons and it tendency to diffuse into absorber leading to the formation of $\text{Cd}_x\text{Sb}_y\text{S}_z$. This phase formed by the CdS compound has been research as an alternative for ETL compounds in photovoltaic cells [40], [41]. In combat of Cd toxicity, TiO_2 emerges as one of the promising non-toxic, stable and abundant ETL materials for the fabrication of solar cells. The properties of TiO_2 that give it an edge include its proper optical transmittance, its alignment with light absorbers and the high electron mobility on this material surface [42], [43]. Therefore, TiO_2 material has been chosen in this study as ETL layer partner for Sb_2S_3 absorber-based solar cell.

1.4 TiO₂ thin films properties

Titanium dioxide (TiO₂) or titania is a highly promising material for semitransparent solar cell fabrication due to its superior structural, morphological and optoelectronic properties. TiO₂ is an inorganic n-type semiconductor material which has shown great applicability in third generation photovoltaic cells. TiO₂ crystal structure comes in mainly two polymorphs tetragonal anatase (space group I41/amd) and rutile (space group P42/mnm). TiO₂ also comes in orthorhombic structure as brookite (space group Pbca). Anatase TiO₂ has lattice parameters $a = 0.54$ nm and $c = 0.95$ nm. Rutile phase possesses lattice parameters $a = 0.46$ nm and $c = 0.30$ nm. The thermodynamically stable rutile phase is also obtained by annealing anatase TiO₂ over 500-600°C[45]–[47]. The presence of TiO₆ octahedra sharing edges and corners is typical for crystalline TiO₂ microstructures. For semitransparent solar cell applications, anatase TiO₂ phase is generally more favourable due to its low surface energy and greater charge transport[48].

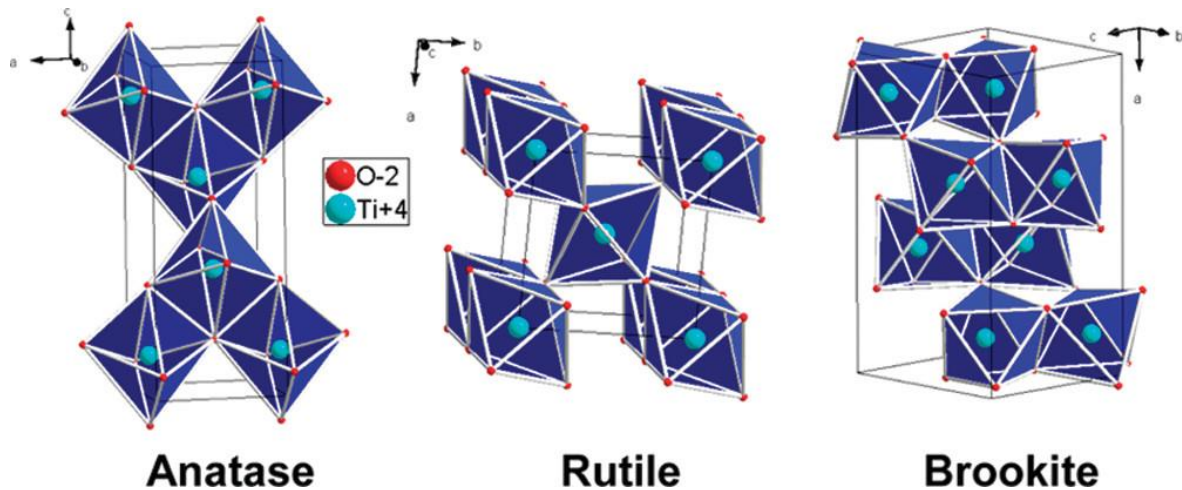


Figure 2. Crystal Structure of Anatase, Rutile, and Brookite TiO₂ Polymorphs [46].

The bandgap of Rutile (110) and Anatase (101) TiO₂ ranges from 3.0 – 3.2 eV. This is particularly important in nanostructure TiO₂ with mixed anatase-rutile phases as it provides possibilities for developing devices with tuneable optoelectronic properties, optimum surface energy, and greater stability[49]. Based on the structure of titania, it is able to be prepared in planar, nanostructure, mesoporous forms, or as nanoparticles through a variety of deposition methods including Atomic Layer Deposition (ALD), Pulsed Layer Deposition (PLD), Chemical Vapour Deposition (CVD), Spray pyrolysis method and other solution-based methods[47], [48].

As TiO₂ film have been deposited by ALD and spray pyrolysis method, the description of the methods will follow in next chapters.

1.5 Thin films deposition methods

1.5.1 Atomic Layer Deposition (ALD)

Atomic layer deposition (ALD) technique is form of chemical deposition requiring the use of cyclic gas-surface reaction to fabricate thin films, especially for it application in solar cells. This form of deposition allows the growth of the precursor vapor on a surface increasing in thickness over time. This advantage in the deposition process gives it an edge of control over the thickness of the film fabricated. This is an important aspect for the design of microelectronic devices a component usually in the nanoscale level. The surface grown using the ALD technique in a self-limiting surface reaction guarantee's that the surface grows at the sub-atomic level layer by layer giving a complete control over the thickness of film as this is just a function of time to build conformational deposited thin films [44].

ALD was developed in the 1970s (then called atomic layer epitaxy) and over the years, Atomic Layer Deposition has been utilized in various applications including electronic devices, solar cells, batteries, and energy storage, [45].

Atomic Layer Deposition relies on usually two complimentary self-limiting reactions that occurs on the surface of the substrate placed in a reaction chamber at special conditions, featuring alternate pulsing and purging of the precursors in the reactor, respectively. This results in (sub)monolayer growth of thin films on the substrate with nanometre precision and the cycle is repeated several times to obtain the desired thickness of the film[46]–[49]. ALD has proven over the years to produce larger-grained, conformal monolayer, high purity films with lower consumption of precursors compared to [50] although at the cost higher vacuum requirement and lower film growth rate per cycle (GPC). In light of the disadvantages of temporal or batch ALD, there has been more efforts to develop spatial ALD which is a continuous process and can be operated at atmospheric pressures [51]. Figure 3 below illustrates a typical ALD process.

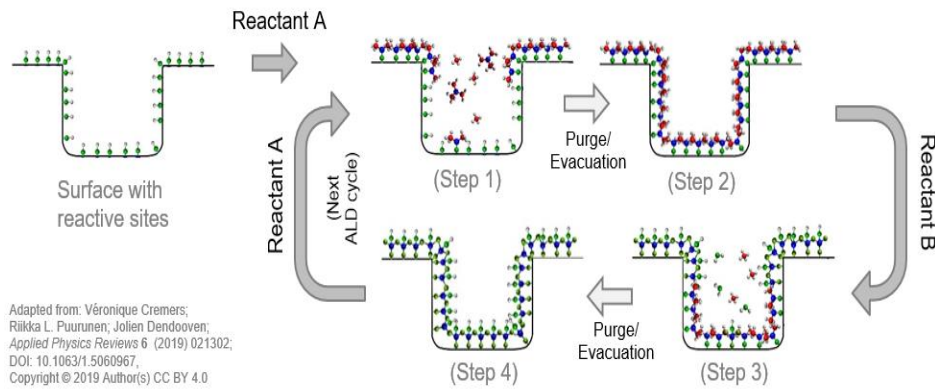


Figure 3. Schematic Showing a Typical ALD Process [52]

Atomic layer deposition process is characterized mainly by the Growth Per Cycle (GPC) in orders of 1 Å/cycle. Films quality is affected by several factors such as choice of precursors, deposition temperature, number of cycles, pulse & purge time, post deposition annealing temperature, etc [53].

1.5.1.1 TiO₂ thin films by ALD

According to a high number of publications on TiO₂ thin films deposited by ALD method, the ALD it could be concluded, that ALD is a one of the most widely used methods to produce TiO₂ thin films. The choice of precursors directly influences the surface chemistry of the ALD processes. Suitable precursors should be sufficiently volatile, possess suitable decomposition temperature, reactive to the other precursors. The compounds TiCl₄, homoleptic halides, alkylamides and alkoxides have all been reported in literatures are precursor of Ti and water vapor and ozone or oxygen plasma as oxygen source. The most widely used precursors are TiCl₄ as titania source and H₂O vapor as oxygen source [54], [55]. The temperature of the process is a key variable in the optimization of the ALD process. Generally, amorphous films get fabricated at lower deposition temperatures which is different from the films with anatase structures which are reported with intermediate temperatures. The mix of the anatase and rutile phase or that of the pure TiO₂ film requires high deposition temperatures for their fabrication within a very short period of time [55].

For the TiCl₄/H₂O process which was explored in this study reports the formation of anatase at the begin on the surface of an amorphous TiO₂ material which has a temperature of 125°C – 165°C or above. The rutile form of the TiO₂ crystals starts to form at a temperature of 350°C or above. The fabrication of thin films via the TiCl₄/H₂O route, the formation of rutile was not seen until temperature of 440°C. In the utilization of oxygen gas plasma as the source of oxygen for the deposition process, lower temperatures are required for crystallization, as anatase was seen by XRD at 135°C and already by FTIR at 110°C [44].

The pulse and purge time of the precursors also affect the ALD process. Lower pulse times may result to underexposure of precursor to active growth sites leading to nodule growth. Increasing the pulse times increases nucleation and growth of the film on active sites till saturation is achieved. At this point a steady growth rate can be achieved. Further increase of the pulse time may not increase the growth rate beyond surface-saturated threshold, but only increase process times and precursor consumption[53].

Another great influence to the nature of the TiO₂ thin films for optical application is the number of cycles. The morphology in terms of thickness of the film, crystallinity and the conformality of the fabricated film is influenced by the ALD cycles number which are tuned also by its adjustment [56], [57]. In Zhang *et al.*, (2017) reports, the structure and crystallinity were impacted by the number of ALD deposition cycles [58]. The particle size of the TiO₂ grains on the film significantly differ; films produced with 60 ALD cycle numbers had a size of 22.1 ± 8.5 nm while that of the uncoated film had a particle size of 20.3 ± 7.7 nm [59].

In a recent work, the effect of ALD cycles on the film thickness of TiO₂ films has been carried out [57].

1.5.2 Ultrasonic Spray Pyrolysis (USP)

Ultrasonic spray pyrolysis (USP) is another deposition technique for the fabrication of thin-layered films [60], [61]. In the USP process, the material-solution to be fabricated in nano-size or to make a thin layer is first atomized ultrasonically [62]. The ultrasonic mist droplets of very fine-sizes are then sprayed into a furnace or pre-heated substrate, where they are thermally decomposed and form a thin film [62, 63]. Figure 4. shows a typical illustration of the USP deposition process.

Unlike the CVD technique which requires a vacuum system which might be expensive to maintain, the USP technique works efficiently under the atmospheric pressure [60], [64]. The USP technique also allows during fabrication for an all-round parameter control, hence enhancing the output material's homogeneity [61], [65]. The controllable parameters in the USP synthesis process include flow rate, precursor's solution viscosity, temperature of deposition, temperature of the substrate deposited upon, the amplitude of the ultrasound among many others [61].

The advantages of this technique (USP) i.e., its operational low cost, tweakable parameters and the absence of a vacuum system has made it a useful concept in the study of photovoltaic cells, photocatalytic and di-electric materials [66]. The critical factors of concern for this process include the rate of spray, the temperature and exposure environment of the substrate for deposition, the transport rate of the gas and its direction [66, 67]. Other factors that do not fall within but are also significant includes the mist droplet size, the concentration of

precursor solution and the evaporation rate of the solvent affects the thickness and crystallinity of the output film [68], [69].

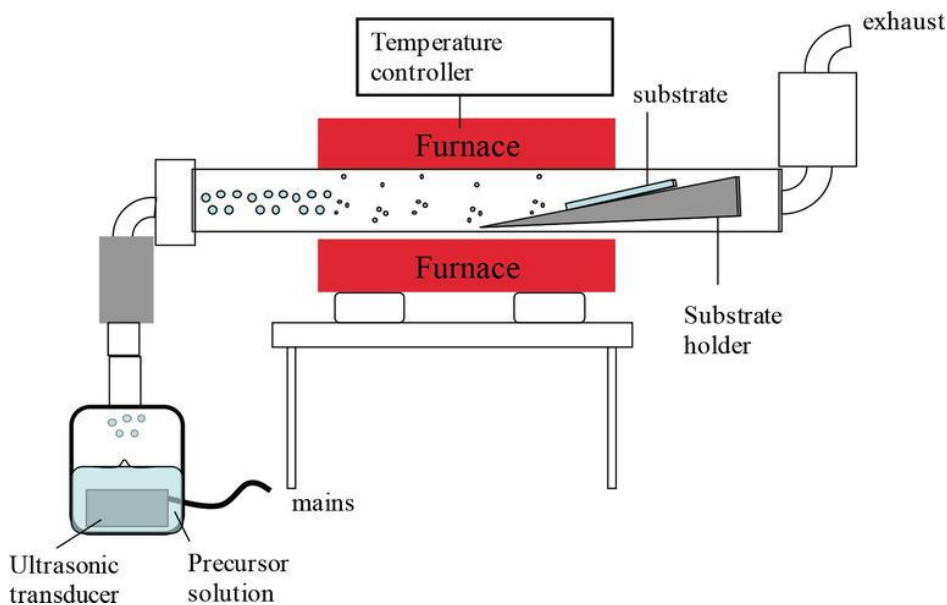


Figure 4. A Typical Ultrasonic Spray Pyrolysis (USP) Deposition Process [70].

1.5.2.1 TiO₂ Thin Films Deposited by Ultrasonic Spray Pyrolysis (USP)

It has been established in literature that the properties of TiO₂ thin films fabricated utilizing the USP technique depends significantly on the process parameters such as; precursor solution concentration, the temperature of the substrate, the distance of the nozzle, the annealing treatment conditions and the spray rate [71]. Morphological properties of the TiO₂ film could be altered by these parameters to give different crystalline phases such as the rutile, brookite and anatase phase, with the anatase phase been the most common with the USP technique [72], [73]. The anatase phase is considered stable thermodynamically at low temperatures (below 600°C) for bulk TiO₂ while the rutile at temperatures above 600°C, therefore for desired crystallinity of the TiO₂ the post-annealing temperature or the temperature of the substrate are tweaked. To achieve the metastable brookite crystalline phase, the precursor solution and its concentration together with the doping process of the TiO₂ is manipulated [64], [74], [75]. The optical properties of TiO₂ thin film fabricated adopting the USP techniques are also tuneable and controllable using variables such as TiO₂ doping level, the crystalline phase of the film and the film's thickness [76]–[78]. The band gap of the TiO₂ thin film can be adjusted and manipulated by changing the material's crystalline phase with rutile having a band gap of 3.0 eV, anatase between 3.2 eV and 3.7 eV, and brookite between 3.0 eV and 3.6 [79]. The growth process of the TiO₂ film from the USP deposition technique utilizes the precipitation process of a selected compound unto a desired substrate material to give uniform thickness, great adherence and a large surface area following the annealing step [70].

The precursor solution concentration effect has been studies on the TiO₂ transparent film

(Anatase-TiO₂) for its applications, and has shown significant correlation with the optical performance and growth kinetics of film [80]. Other related studies of dependent on parameters of TiO₂ films for application in solar cells utilizing the USP technique include a study by Arunachalam *et al.*, (2015), where the TiO₂ was deposited onto an ITO substrate using the spray pyrolysis technique. The effect of different substrate temperature was investigated, with 450°C favouring the formation of the TiO₂ anatase phase and 475°C favouring the TiO₂ rutile phase of crystallinity. Further results from this study reported a transmittance level above the 85% mark making it a viable material for solar cell application [81].

2. CHARACTERIZATION METHODS

2.1 Thin Films Characterization Techniques

2.1.1 Scanning Electron Microscope

The scanning electron microscope is an imaging technique that uses to scan the surface of material and produce high-resolution (down to 5 nm) images and detailed information about morphology and topography of the specimen. SEM can reveal the tiny features that are much smaller than those visible with optical microscopy [82].

Sometimes SEM can be utilized to estimate the thickness of the sample, through analyzing a cross section of the sample. The specimen is irradiated by high energy electron beam which interacts with the atoms in the sample, causing them emit different types signals, such as secondary electrons, and backscattered electrons. Emitted electrons represent a detailed visual image of a sample with high-quality and spatial resolution. Coupling the scanning electron microscopy with the energy dispersive x-ray (EDX) utilizing similar principles can additionally detect the elemental composition of material surfaces [83]. Figure (5) below depicts the schematic of the scanning electron microscope showing its make-up components;

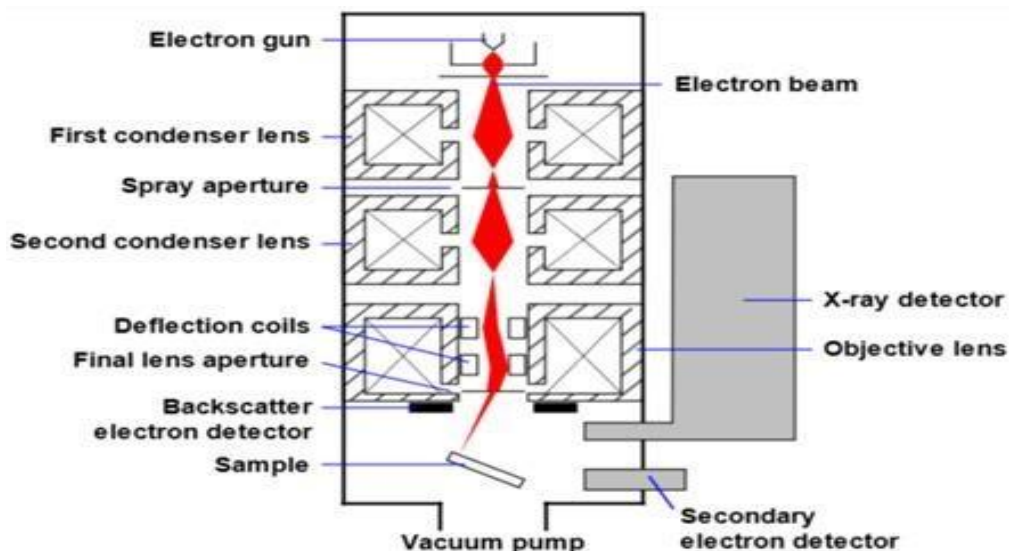


Figure 5. Schematic figure, showing the components of a Scanning Electron Microscopy [84].

The schematic of the scanning electron microscope showing the different component of the imaging instrument contains primarily the electrons source, electromagnetic lenses, sample chamber, control unit and the detector for electrons [85], [86]. The production of electrons starts at the top of the column which is forced down and passed through magnifying lenses and different apertures aiding in the focusing of accelerated electrons to the specimen on the slide to be viewed. The characterized sample is placed such that it is centered to receive the accelerating electrons, this part is labelled the chamber area. The electron chamber is usually equipped with pumps to produce a high-pressured vacuum [86]. The SEM and EDX techniques are primary methods to study solid state matter materials nowadays.

2.1.2 UV-Vis Spectroscopy

This technique for material characterization is measured either as transmittance or absorbance of photons (radiation energy) which is a unique property of all material at different wavelength of light [87]. There exists a relationship between the transmittance of a given material and its optical band gap in electron volts [88]. This technique is classified quantitative in nature since it effectively measured the absorbed or transmitted radiation energy of a given chemical species. It has shown its application in near all sample phases (solid, liquid and gas) and cover the measurement of the radiation form the ultraviolet region of the light spectrum (100 to 400 nm) and the visible light region (400 to 800 nm). The principle of operation for this technique is in the measurement of intensity of light passing through a considered sample and its reference. Figure (6) gives an illustrative schematic showing the UV-Vis measurement process using integrated sphere models. The reading forms the UV-Vis spectrophotometer

such as the reflectance, absorbance and transmittance reading translates to the measurement of solar thin films thickness, band gap and other optical parameters that helps to effectively assess the optical parameters of the fabricated solar cell [87], [88].

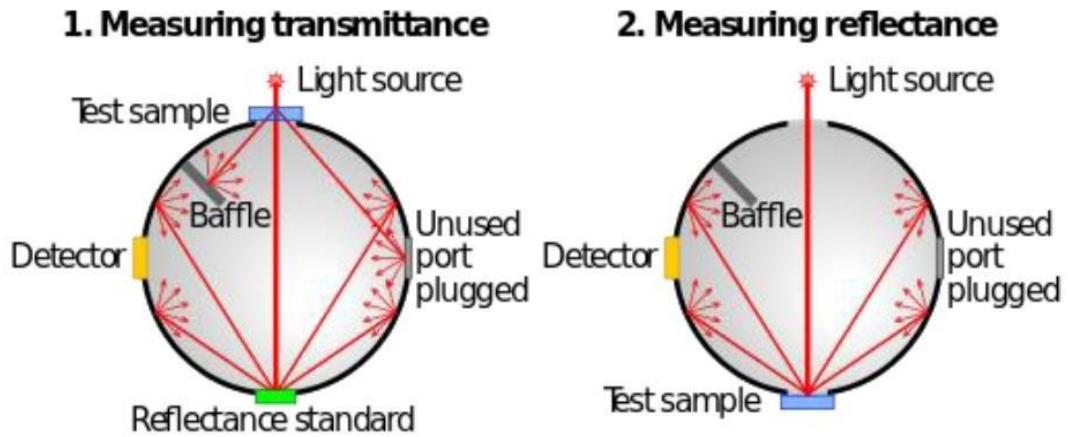


Figure 6. UV-Vis spectrophotometry showing the different modes of measurement (Transmittance and Reflectance) [84].

To calculate the transmittance and reflectance value of a given material from the absorption of the material of the spectrum of light, the intensity of the radiation divides the measured transmitted or reflected radiation measured or gotten from the absorbance value [87]. The formula that carries the function obtains the absorption co-efficient (α) as expressed in equation (1);

$$\frac{T}{100-R} = e^{-\alpha d} \quad \text{Eqn. 1}$$

Where; T is the transmittance, R is the reflectance, d is the thickness of the film. To further reveal more information from the UV-Vis spectroscopy, the optical band gap is also measured; this measurement is done using the Tauc equation relating the band gap and the absorption coefficient. This shown below as equation (2);

$$(\alpha h\nu)^n = A(h\nu - E_g) \quad \text{Eqn. 2}$$

From equation (2), h is the Planck's constant, ν is frequency of irradiation absorbed, A is a constant and E_g is the optical band gap [89].

2.1.3 X-ray Diffraction

The XRD technique provides information about crystallinity, phase, size, strain of molecules, surface texture, crystal defects and orientations [90]. The principle of operation for this technique is tied to the ability of light to diffract i.e., to elastically scatter on a surface with measurable angles. Photons from the x-ray source is scattered periodically according to the lattice arrangement of the solid surface which in turn forms a constructive interference

showing a pattern in the arrangement of atoms or crystal grains on the surface of the material [91].

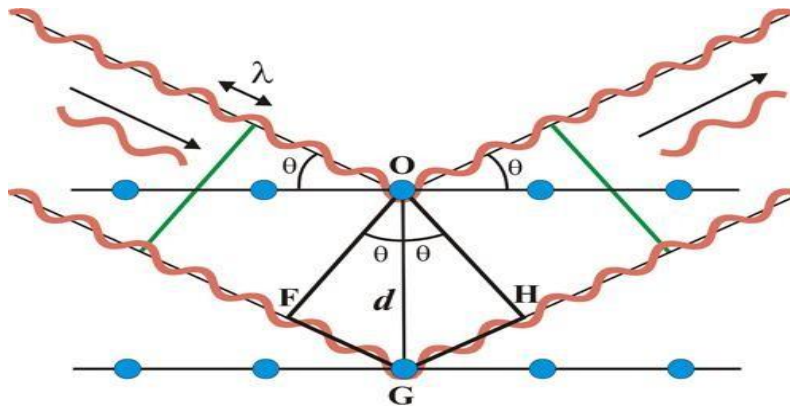


Figure 7. Working Principle of the X-ray Diffraction Characterization Technique [92].

Figure 7 depicts the light scattering and constructive interference on the surface of the material from the monochromatic radiation source illustrates using a single crystal plane the Bragg's law which is expressed as a measurable quantity as equation (3) below [91];

$$n\lambda = 2d \sin \theta$$

Eqn. 3

from the equation (3), θ is the angle measured in-between the incidence ray and the normal of the reflected ray on the crystal lattice plane, λ is the x-ray wavelength, d is the atomic spacing of the crystal grains while n is the order of reflection which are whole positive integer. Using the equation (3), the measurement of the angles between the incidence and reflected beams on the normal represented as θ , the distances between the atoms or grains that makes up the crystal individually is known as d . Therefore, once the distances of every phase of the crystal is known and measured the morphological pattern and arrangements is then revealed. A diffractometer is used in the measurement of the diffraction pattern on the surface of the solid-state material or with the help of a record photo-camera; it is from this device that a list of the diffraction line, their intensities, angles and the measured d -spacing are prepared. The prepared list is then compared with standard list of compounds in an archive known as the powder diffraction file (PDF). This database contains a number of different compounds and their diffraction patterns. The database is managed and reviewed annually by the international centre for diffraction data (ICDD).

2.2 Solar cells characterization techniques

2.2.1 Current voltage characteristics

The current-voltage (J-V) technique stands out the major and important technique in the characterization of solar cell performance. This technique capitalizes on the production of current by the solar cell under irradiation which is also term the photovoltaic effect acting similar properties as that of a diode [93]. The concept begins with the flow of electrons via the p-n junction which is classified as generation of electrical charges with a reduced electrostatic force on the surface of the material. The diode generated current flow opposite and parallel to the electron flow which also tagged a 'reverse current'. The solar cell which biases itself makes both a positive and a negative bias (greater than or less than zero). Under positive bias the reverse current rises exponentially while under negative bias it is negligible for measurement [94]. Equation (4) shows an ideal model for the diode current measured as external photo- generated-current in short circuit systems;

$$J(V) = J_0 \left(e^{\frac{qV_{bi}}{k_B T}} - 1 \right) - J_{sc} \quad \text{Eqn. 4}$$

Where; k_B = Boltzmann constant, J_0 = reverse saturation current, V_{bi} = applied bias in V, T = the temperature in kelvins, J_{sc} = a short circuit current density which is measured in mA/cm² [93], [95]. To calculate for the open-circuit voltage (V_{oc} , V) it is important to note that it is generated at the maximum positive bias of the solar cell. This is recorded when the solar cell is under irradiation but not connected to an external circuit. Equation (5) shows the mathematical expression to calculate for this;

$$V_{oc} = \frac{kT}{q} \ln \left(\frac{J_{sc}}{J_0} + 1 \right) \quad \text{Eqn. 5}$$

Where; k = Boltzmann constant, T = the temperature in kelvins, J_{sc} = the short circuit current density which is measured as mA/cm², q = elemental charge in C and J_0 = the reverse saturation current [93]. Another parameter important in measuring the squareness of the solar device which impacts strongly the current density-voltage is the fill factor. The measure of the fill factor accounts for the series and shunt electrical resistance on the surface of the solar film which may impede current flow. A good result for the fill factor shows a low series resistance which infers the flow of charges on the material surface without much resistance; while the shunt resistance clearly reveals areas on the film surface that act parasitically on generated electron flow. An example of the shunt resistance is the connecting route of the surface of the material with front and back contacts. The fill factor ratio should be large enough

to accumulate higher photocurrent externally [93], [94]. This ratio is shown in equation (6);

$$FF = \frac{J_{mp} \times V_{mp}}{J_{sc} \times V_o} \quad \text{Eqn. 6}$$

Where; V_{mp} = the maximum point for voltage in V, J_{mp} = the maximum point for current density which is measured in mA/cm², V_{oc} = open-circuit voltage and J_{sc} = short circuit current density. The current density-voltage measure as shown on the plot in figure (8), which for individual solar devices are measured for under irradiation and in the dark holds information when bias is introduced. In ideal state without irradiation- dark phase (forward bias active) there is only the diode current. Under irradiation- illumination phase there exist the external photocurrent leaving the diode current with a negative value as shown in equation (7) calculating the power density of the solar device; where the maximum power points are tagged V_{mp} and J_{mp} on the current density-voltage curve (J-V curve). Additionally, to calculate for the photoconversion the equation (8) is applied denoted as PCE and as η . This parameter is held as the main feature under characterization of the solar cell. The PCE shares a relationship with the power density for the solar film as expressed in the equation (19), where P_s = the irradiance measured in W/m² [93], [94].

$$P = FF \times J_{sc} \times V_{oc} = J_{mp} \times V_{mp} \quad \text{Eqn. 7}$$

$$PCE = \frac{J_{mp} \times V_{mp}}{P_s} \quad \text{Eqn. 8}$$

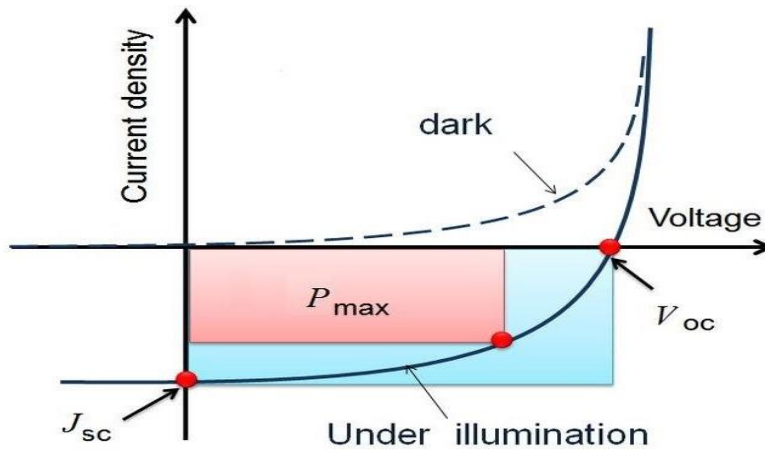


Figure 8. Current density-voltage performance of a solar cell in the dark and under illumination [94], [96].

2.2.2 Kelvin Probe Spectroscopy (KPS)

The Kelvin probe spectroscopy is a surface characterization technique which operates on the non-contact mode where work functions are assigned to both the sample surface and the instrument's cantilever tip [97], [98]. The tip and the sample bear an electrical charge

relationship such that as they are brought close together, they generate a net electrical current which is measurable until alignment with the fermi levels. The conducting instrument's tip height which bears a work function can then be compared with that of the work function of the sample surface. The difference in these work functions (between the tip and the sample) is described as the contact potential difference (CPD) which does well in giving describing the surface nature of the sample measured [99].

Other than the atomic force of attraction or repulsion that exist between the instrument's tip and the sample surface, they also share electrostatic forces. It is the measure of the electrostatic force between them that accounts for the CPD of the surface material. To measure this, the cantilever of the instrument which holds a reference electrode which forms a capacitor with the material's surface [100]. To take measure of the CPD of the sample surface, known voltage is passed through the established circuit of the tip and sample. This voltage passed consists of a direct current bias (V_{DC}) and the AC voltage ($V_{AC} \sin(\omega t)$) with a certain frequency (ω). the detection of the electrostatic force between the tip and the sample is done by passing an alternating current voltage to the instrument's tip and fixing in place a lock-in amplifier [100], [101]. To restrict mix signals (electrical and topographic), the AC voltage is set most often at the second resonant frequency or distant from the first resonant frequency. Equation 9, further explains this mathematical relationship;

$$V = (V_{DC} + V_{CPD}) + V_{AC} \sin(\omega t) \quad \text{Eqn. 9}$$

Where, V_{CPD} = contact potential difference.

Furthermore, the electrostatic force is calculated by differentiating the energy function as shown in equation 10;

$$F = \frac{1}{2} \frac{dC}{dz} V^2 \quad \text{Eqn. 10}$$

Where, C = Capacitance, z is the separation and V =Voltage, each of the parameter belong to the tip and each point of the sample surface. This setup is illustrated as figure 9.

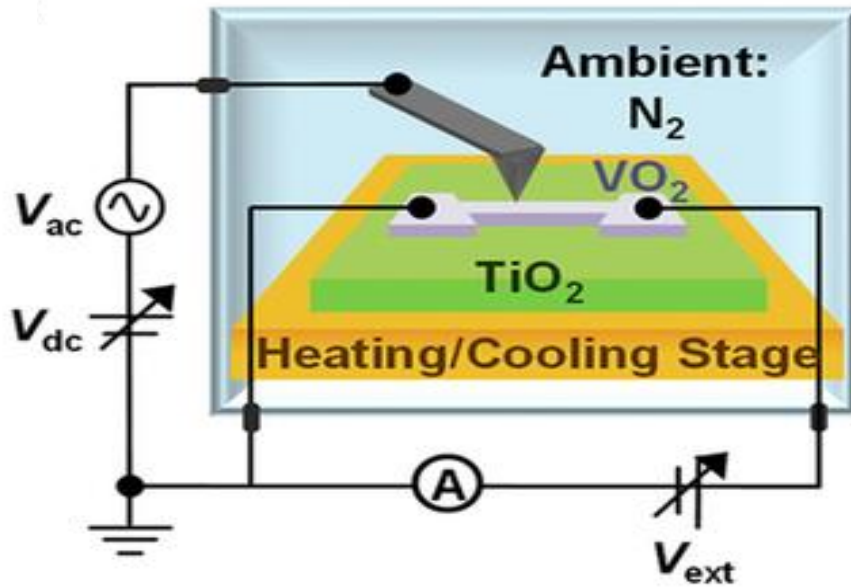


Figure 9. Schematic illustration of the transport and Kelvin probe force microscopy (KPFM) measurement setup [102].

2.2.3 Photoemission Yield Spectroscopy (PYS)

Photoemission Yield Spectroscopy (PYS) is a method used to characterize materials, particularly in the context of organic materials and thin films. It measures the number of photoelectrons as a function of incident photon energy [103]. In a vacuum system the PYS process consist of three basic steps, which induce; (a) the excitation of electrons optically, from a lower-ground state to higher energy state (b) the transport of these excited electrons to the surface of the material (c) the electron escapes from the material's surface into the vacuum system [103]. There exists an inelastic scattering effect that occur during the transport of primary electron from the surface of the material to the vacuum, also, during this step the secondary electron at low energy states kinetically get excited [104].

The electrons which escape into the vacuum space are trapped a utilized by a created moderate electrical field; this done to avoid the creation of negatively charge space near the surface of the sample under analysis. Under ambient external parameters the electrical current is replace with an ionic one which is recorded [104], [105]. Additionally, in air electrons which escape from the surface of the material and possess a mean free path $<1 \mu\text{m}$ gets attaches to the particulate and molecular constituent of air (Oxygen, nitrogen and water vapour), therefore chemically forming negatively charged ions [106]. This phenomenon leads to the production of anions with higher mean free path, which has more drift power than the primary electrons, thus finding it way through the medium to the positively charge electrode. This migration of charges is what accounts for the measure of photoelectron current [106], [107].

The PYS technique for the characterization of metallic surfaces and the determination of their work function together with the ionization energy of semiconductor materials is centred around the accurate measure of the sample's photoelectron yield. The photoelectron yield is defined as the count of photoemitted electrons from certain material surface per an incidence photon at a specific photon energy ($h\nu$). The photoelectron yield which is a function of photo energy has a relationship with the ionization energy as photoemission of electron is only possible when the photon energy is greater than the threshold ionization of the sample surface [108], [109]. Equation 11 below expresses this mathematically;

$$Y(h\nu) \propto (h\nu - E_i)^n$$

Where, Y = photoelectron yield, E_i = the threshold ionization energy for the sample material and n = the power index. The variable $n=2$ is used for metal and semiconductors (degenerate), $n=3$ is for most inorganic semiconductor samples when considerations are made on the sample volume excitations, while $n=1, 3/2, 5/2...$ are for semiconductor samples when considerations are made on the band state of the material or its surface imperfections [109]. $n=3$ power index is used by many organic semiconductors as it is also the case of all inorganic ones therefore, to determine the E_i value we check for the threshold on the $h\nu$ - Y^n plot. Other than the ionization energy information provided by the PYS spectra, information about the effective density of states from the fermi-level to $h\nu - \Phi$ below E_f is revealed [108]–[110].

3.RESULTS AND DISCUSSION

3.1 Experimental

Solar cells used for this study were fabricated with the configuration FTO/TiO₂/Sb₂S₃/P3HT/Au as depicted in Figure 10 below.

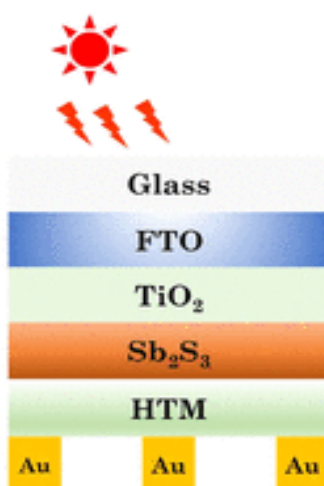


Figure 10. Solar Cell Structure Used in Study

18 x 18mm Glass substrates coated with flourine-doped tin oxide (FTO) layer (Alfa Aesar) of 300nm thickness and 7 Ω /sq sheet resistance were used as substrates to grow TiO₂ films. The substrate preparation includes cleaning with detergent solution and isopropanol, washing with double deionized water, and drying in air. The clean samples were also treated with UV-C light illumination for 30 minutes.

3.1.1 Thin Film Deposition

TiO₂ ETL layers for this study were deposited by two techniques; atomic layer deposition (ALD TiO₂) and ultrasonic spray pyrolysis (USP TiO₂).

ALD TiO₂ thin films were deposited using model R-200, PICOSAN ALD machine. Precursors of TiCl₄ and DE water were used for this deposition. The deposition occurred at 125°C. For the TiCl₄, the volumetric flow rate was 150 sccm, 0.1 second pulsing and 3 seconds purging time. For DE water, volumetric flow rate was 200 sccm, with pulsing and purging time of 0.1 and 4 seconds respectively. As earlier established, ALD TiO₂ film thickness is influenced by the number of cycles. This, in addition to SEM cross sectional images, was used as a control

parameter in adjusting for film thickness. 100, 200, 400, 800, and 1000 ALD cycles were used in this study, resulting to film thickness of 5, 15, 30, 60, and 75nm respectively. Post-deposition annealing in air at 450°C for 30 minutes were performed on all samples. Prior to deposition, a 3 mm wide strip of heat resistant Kapton® tape was glued onto the FTO side to preserve access to the back contact.

In order to deposit USP TiO₂ films, precursors consisting of a solution of 0.1 mol/L titanium tetraisopropoxide (TTIP) and 0.4 mol/L acetylacetonone (AcAc) dissolved in ethanol were sprayed on glass/FTO substrates maintained at 450°C in air.

Sb₂S₃ absorber layer has been deposited by USP from mixture 0.1 mol/L SbCl₃ and thiourea (molar ratio of 1:3) of thiourea at 200 °C with a nebulization frequency of 1.7 MHz and a power of 200 W. Polythiophene, P3HT, was used as a hole conductor material and was deposited by spin coating technique on a top of Sb₂S₃ layer.

3.1.2 Thin film and SC Characterization

A Zeiss HR FESEM was used to examine the surface and cross-sectional morphologies of the layers. The optical absorption and transmittance measurements were made using a Jasco V-670 ultraviolet-visible spectrophotometer (UV-VIS) in the range of 300–1000 nm. Taucs model was used to determine the band gaps of TiO₂. The phase composition and structure were characterized by X-ray diffraction (Rigaku Ultima IV, Si strip detector D/teX Ultra, 0-20, CuKα₁, λ=1.5406 Å, 40 kV, 40 mA, 5° min⁻¹, step 0,02°). A texture coefficient of the Sb₂S₃ absorber layers were calculated in accordance with equation (12).

$$C_{hkl} = \frac{I_{hkl}/\Sigma I_{hkl}}{I_{hkl,ref}/\Sigma I_{hkl,ref}} \quad (12)$$

Where C_{hkl} is the texture coefficient, I_{hkl} the measured intensity from Sb₂S₃ XRD pattern, $I_{hkl,ref}$ the reference powdery Sb₂S₃ intensity of each detected crystallographic growth direction corresponding to the Miller indices [28].

Work function (Φ), ionization energy (E_i) and the energy difference between Fermi level (E_F) and valence band maximum (E_{VBM}) of the TiO₂ films were measured by PYS and KP techniques on ambient-pressure KP Technology SKP5050-APS02 instrument. The current-voltage (I - V) characteristics of the fabricated solar cells were recorded using Wavelabs LS-2 LED solar simulator with an AM1.5G (100 mW cm⁻²) light source.

3.2 Results

3.2.1 Structural and Optical Properties of ALD and USP TiO₂ Layers

To investigate the phase composition and structural property of the ETL layers of the fabricated TiO₂; the thicker layers were deposited on Glass/FTO substrates. An annealing temperature of 450°C was applied as condition for its synthesis. This approach made it similar to that of the synthesis conditions of the TiO₂ thin films fabricated. Figure 11 represent the XRD pattern for the annealed TiO₂ layer carried out using ALD and USP techniques. Reflection 2theta peaks at 25.35 and 37.96 showed dominance while, those at 11°, 38.68°, 48.08°, 54.10°, 55.30 °and 62.85° which corresponded with the crystal index (101), (004), (103), (112), (200), (105), (211) and (204) respectively- indicated an anatase TiO₂ surface morphology [111]. There were no records the material crystal peaks revealing any other crystal structure types other than anatase [111], [112]. This reported result is similar to some previous investigation on thin film morphology, with the anatase phase appearing solely in the XRD patterns [111]- [113].

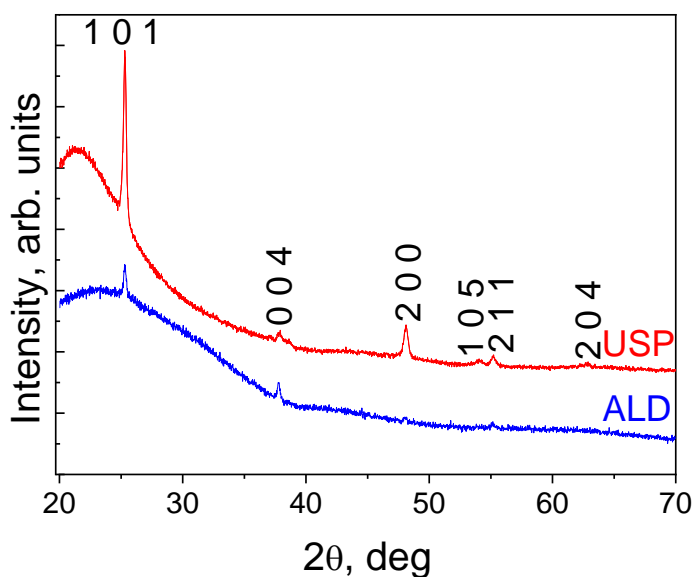


Figure 11. XRD pattern of USP and ALD TiO₂ films annealed at T=450 °C.

The Band gap (E_g) results for both USP and ALD deposited TiO₂ film showed a slight difference when compared, with that of USP having 3.35eV and ALD having 3.30 eV. The E_g result from the study is also in line with previous work with E_g ranged from 3.25 to 3.35 eV [114].

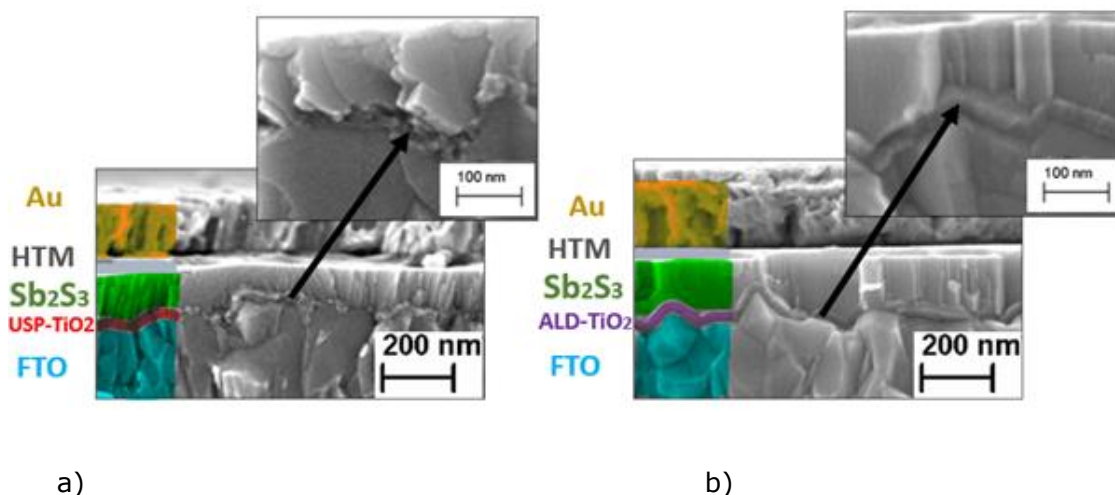


Figure 12. HR- SEM cross-sectional images of FTO/TiO₂/Sb₂S₃/ stack with a) USP TiO₂ and b) ALD TiO₂

Figure 12, graphically shows the cross-sectional image (HR-SEM) of the fabricated thin layer film (FTO/TiO₂/Sb₂S₃/ stack) deposited using the USP and ALD techniques. The TiO₂ films formed appears to be uniform and dense, regardless of if ALD or USP techniques are employed. The range of this layer thickness differ slightly in both USP and ALD technique utilized. ALD-TiO₂ thickness was found to be 30 nm (from 400 cycles) while the USP-TiO₂ layer was in the range of 35-40 nm. The SEM images also proved that the relationship between thickness of TiO₂ film and the number of cycles is a direct one with except to the first 100 cycles which serves as an incubation period. The first 100 cycles produce a thickness of 5 nm, that of 200 cycles produces 15 nm film, 400 cycles then produced 30 nm thickness of film. This theory is common in the investigation of thin films deposited and grown using the ALD Technique [115].

To investigate the interference of the Sb₂S₃ absorber layer's structural properties by the ETL layer of the TiO₂ thin film, the XRD spectroscopy was utilized. The patterns of the XRD for the Sb₂S₃ absorber layer grown on TiO₂ was investigated further to get their texture coefficients. Results from this investigation revealed the interference of the Sb₂S₃ layer by the growth method of the ETL on the TiO₂ thin films. The XRD patterns studies is represent on figure 13b, showing the texture coefficients patterns, which shows a dependence corelation of the Sb₂S₃ absorber layer growth to that of the ETL layer growth method on the film. The texture coefficient corresponding to the (130) plane when the USP deposition method was utilized has shown to be significantly more dominant ca. 5.5 folds (1.1 vs 0.2) than its counterpart texture coefficient deposited using the ALD technique. This finding is confirmed again the comparism

for the texture coefficient corresponding to the (211) plane which appears to be 2 folds larger (1.45 vs 0.7) in the Sb₂S₃ absorber layer USP method than that of ALD technique for the TiO₂ thin film.

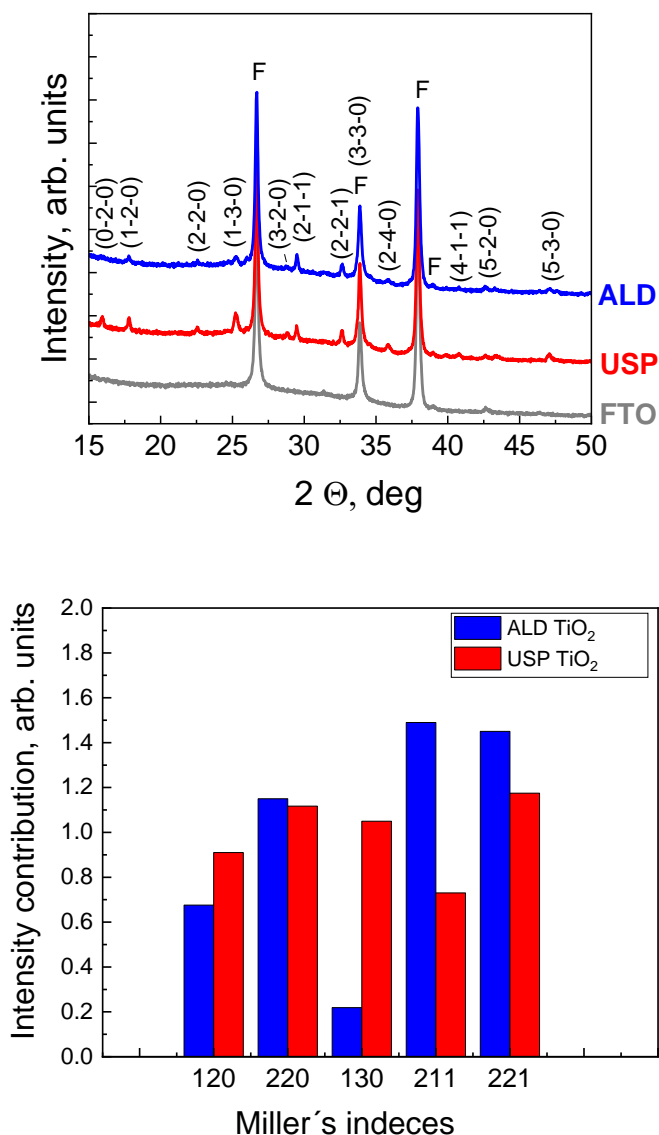


Figure 13. a) XRD patterns and b) texture coefficient values of Sb₂S₃ layers grown on USP and ALD TiO₂ layers

The orientation of the ETL layer has been reported to significantly alter the desired orientation of the Sb₂S₃ absorber layer in previous studies[116]. From this report, the orientation of the Sb₂S₃ absorber layer which was randomly deposited on the ZnO ETL (z-ZnO) gave the preferential orientation (221), this was not so with the orientation deposited on exhibited (001) oriented- ZnO ETL layer[116]. This study aligns with previous observations concerning

solar cell performance. It highlights, in particular, the ideal absorber layer orientation for maximum effectiveness. Notably, the (120) orientation is identified as an inert plane with a low density of dangling bonds. This property greatly reduces interfacial energy, in contrast to Sb_2Se_3 films that are (221) orientated. Because of their large number of dangling bonds, the latter are considered thermodynamically unfavourable and exhibit poor adherence to ZnO surfaces[116]. This is consistent with recent research that found higher efficiency in Sb_2S_3 -based semi-transparent solar cells, approximately 6.6%. Sb_2S_3 thin films with higher ratios of (020) and (120) peak intensities were associated with these efficiencies[116], [117]. Examining the structural factors influencing performance, this research validates these conclusions. We discovered that the USP TiO_2 ETL layer, which is distinguished by higher ratios of (120) and (130), provided superior solar cell performance compared to the ALD TiO_2 films. The latter demonstrated dominance in the (211) and (221) indices, consistent with the studies previously referenced.

3.2.2 SC Output Parameters

In Figure 14, the performance of solar cells (SCs) with TiO_2 layers is shown by the photovoltaic metrics (V_{oc} , J_{sc} , FF, Efficiency, R_{Sh} , and R_s). These layers were created using the USP technique and ALD in different thicknesses. The data clearly shows that the thickness of the ALD TiO_2 layer has a major effect on the output characteristics of solar cells. It turns out that the thickness of 100 cycles, or around 5 nm, is not enough to prevent charge carrier recombination. As a result, in comparison to thicker ALD films, output properties such as V_{oc} , FF, and R_{Sh} are noticeably lower.

Approximately 15–30 nm thick (200–400 cycles) thicker ALD films exhibit improvements in a number of characteristics, including greater V_{oc} (650 mV), increased currents (about 12 mA/cm^2), FF of about 36%, and R_{Sh} ranging from 250–300 $\text{Ohm}\cdot\text{cm}^2$. As a result, efficiency levels are about 3%. In comparison to other thicknesses, the maximum solar cell performance (about 3.3% efficiency) is achieved at an ALD TiO_2 thickness of around 30 nm (400 ALD deposition cycles), which is shown to be the ideal thickness for the highest output characteristics. However, there is a discernible decrease in the values of R_{Sh} , fill factor, and short-circuit current when the ALD TiO_2 films are thicker (800 cycles and above, exceeding 60 nm). As a result, solar cell efficiency is reduced to about 2-2.5 percent.

USP-deposited TiO_2 differs from ALD TiO_2 in that the former has a denser structure as a result of the deposition process, and as a result, smaller currents because of higher resistance. 3 to 4 % SC efficiencies are obtained with larger V_{oc} , J_{sc} , and FF values. This result is in good agreement with a number of recent studies on ALD TiO_2 in solar cells of the perovskite type [116], [118]. It shows that thickness is a key factor in affecting solar cell efficiency and emphasizes the need of adjusting TiO_2 thickness for particular types of solar cells. When

compared to the best ALD deposited TiO₂ SC sample, the performance of the SC based on USP deposited TiO₂ ETL layer is marginally superior.

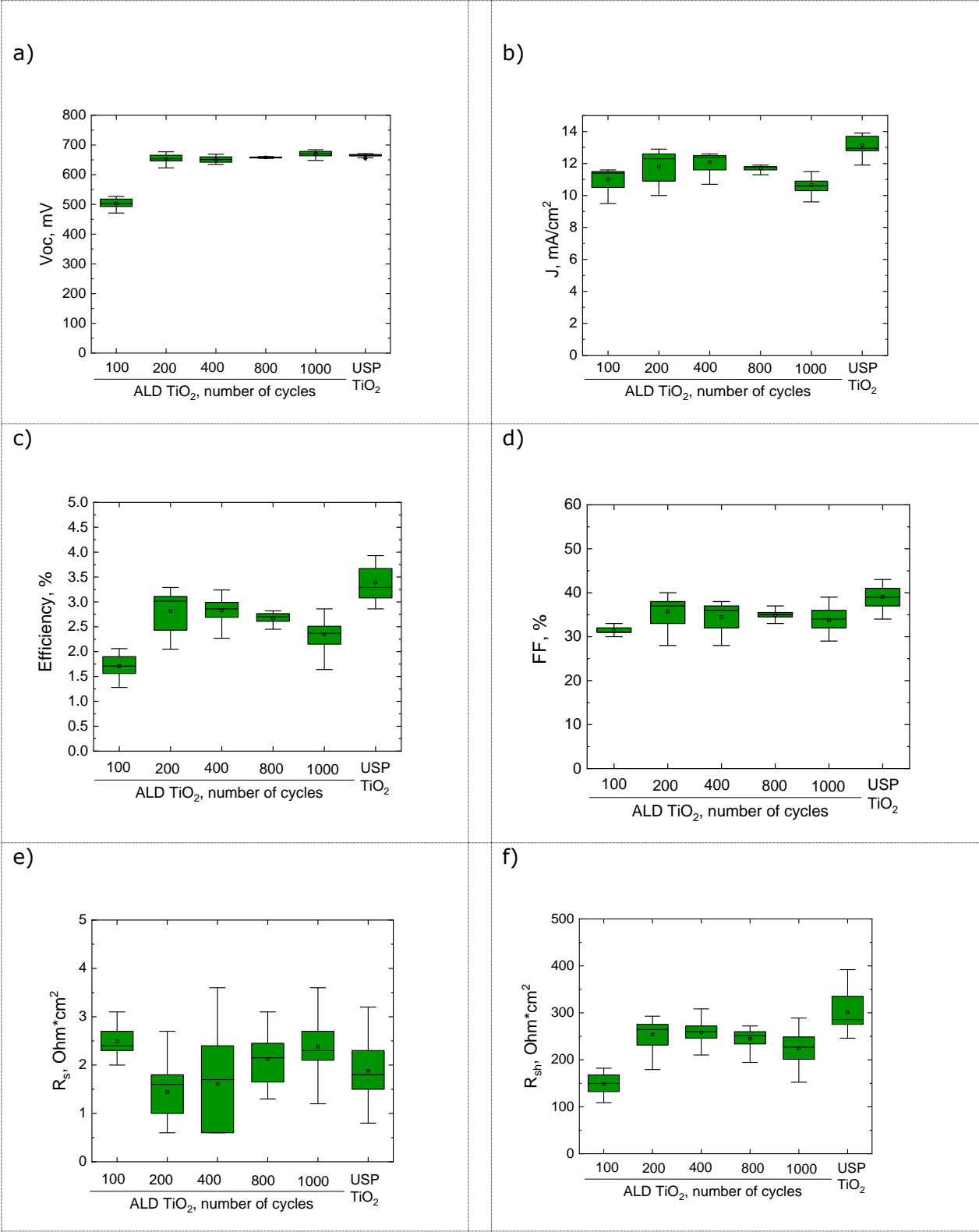


Figure 14. Output parameters of SC with ALD and UPS TiO₂ a) V_{oc} , b) J_{sc} , c) FF, d) Efficiency, e) R_s , f) R_{sh}

3.2.3 Electronic properties and band alignment of SC components in SC structure

Kelvin probe (KP) and photon yield spectroscopy (PYS) techniques were used in the study to investigate the FTO/TiO₂/Sb₂S₃/P3HT/Au heterojunctions. Figure 16 shows the surface photovoltaic (SPV) results, and Figure 15 shows the work function data. Particularly, it was discovered that under dark conditions, the work functions of TiO₂ were 4.18 eV and 4.05 eV, respectively, meaning that the SPV values for USP and ALD TiO₂ were -539 mV and -535 mV. No matter how TiO₂ was prepared, the ionization energy (E_i) recorded by PYS was always 4.84 eV. The valence band maximum (EVBM) in relation to the Fermi level (E_F) was calculated by subtracting the ionization energy (E_i) from the work function (Φ) in order to build the band diagram of these heterojunctions [119]. Furthermore, the conduction band minimum (ECBM) was calculated using the bandgaps of USP-grown Sb₂S₃ and ALD-grown TiO₂ (3.30 eV), as follows: ECBM = EVBM + E_g (3.35 eV). The energy band diagram for the FTO/TiO₂/Sb₂S₃/P3HT/Au heterostructure, shown in Figure 17, was made possible by these computations.

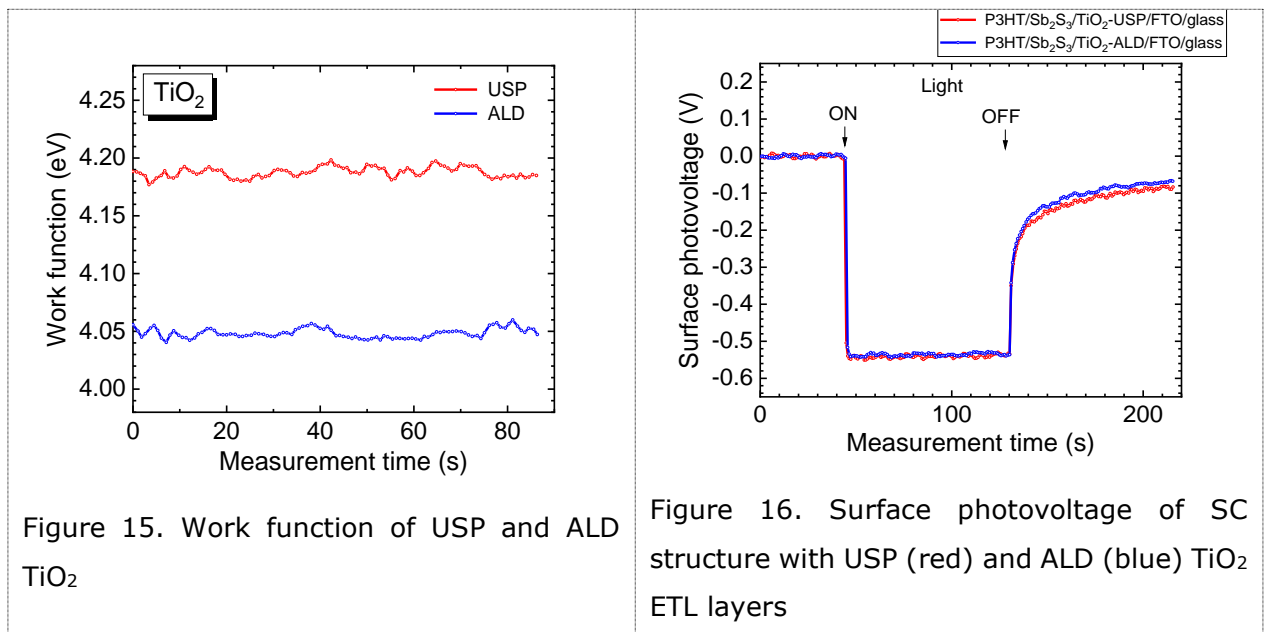


Table 1. Summary table on electronic properties (E_g , SPV, Φ , E_i , $E_F - E_{VBM}$ and $E_{CBM} - E_F$) of SC component layers

| Sample | Top layer E_g (eV) | SPV (± 3 mV) | Φ (± 0.04 eV) | | E_i (± 0.03 eV) | $E_F - E_{VBM}$ (± 0.05 eV) | | $E_{CBM} - E_F$ (± 0.05 eV) | |
|---|----------------------------|-------------------------|-------------------------------|-------|------------------------------|--|-------|--|-------|
| | | | dark | light | | dark | light | dark | light |
| FTO_lit. data | | | 4.30 | | | | | | |
| ALD-TiO ₂ /FTO/glass | 3.30 | 0 | 4.05 | 4.05 | 6.86 | -2.81 | -2.81 | 0.39 | 0.39 |
| USP-TiO ₂ /FTO/glass | 3.35 | | 4.18 | 4.18 | 6.86 | -2.67 | -2.67 | 0.68 | 0.68 |
| Sb ₂ S ₃ /ALD-TiO ₂ /FTO/glass | 1.70 | -277* | 4.79 | 4.51 | 5.43 | -0.64 | -0.91 | 1.07 | 0.79 |
| P3HT/Sb ₂ S ₃ /ALD-TiO ₂ /FTO/glass | 1.9 | -535** | 4.70 | 4.17 | 4.84 | -0.14 | -0.67 | 1.76 | 1.23 |
| Au/P3HT/Sb ₂ S ₃ /ALD-TiO ₂ /FTO/glass | | -491** | 4.74 | 4.25 | 4.74 | 0 | -0.49 | 0 | -0.49 |

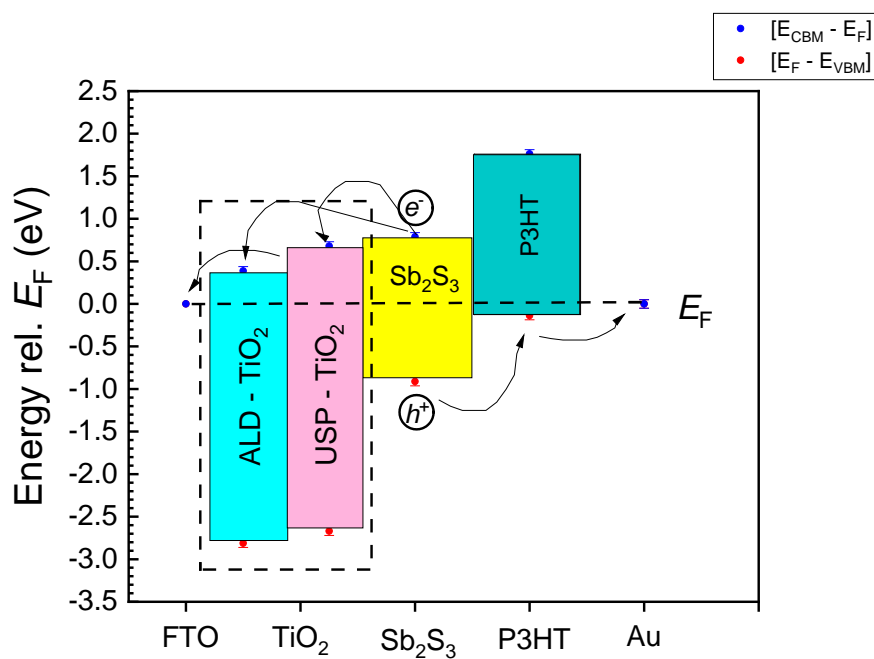


Figure 17. SC band diagram with ALD (blue box) and USP (rose box) TiO₂ ETLs.

The conduction band minimum (CBM) of USP TiO₂ is 0.39 eV greater than that of atomic layer

deposition (ALD) TiO₂, according to the computed band diagram shown in Figure 17. Specifically, earlier studies [79] showed that the power conversion efficiency (PCE) of the solar cell (SC) can be increased to more than 20 percent with a variation of 0.50 eV above the CBM position of the electron transport layer (ETL). A known correlation suggests that more efficient separation of photogenerated electron-hole pairs and a significant decrease in charge carrier recombination occur when the ETL's CBM position is very near to or slightly higher than the absorber layer's, a phenomenon known as a "spike type offset" [120]. This ultimately results in higher open-circuit voltage (Voc), short-circuit current density (Jsc), and FF values (fill factor).

Therefore, the more appropriate CBM band position of the former, which aligns closer to the CBM of the Sb₂S₃ absorber layer, is responsible for the greater SC output characteristics of the USP TiO₂ ETL layer in the solar cell when compared to ALD TiO₂. By facilitating improved electron-hole pair separation and reducing charge carrier recombination, this alignment raises the solar cell's overall efficiency.

Research on titanium dioxide (TiO₂) has yielded varying stated work function values. The value of 4.18 eV for USP TiO₂ is in close agreement with the 2.23 and 4.20 eV values for spray pyrolyzed TiO₂ that have been published by other researchers [79]. The conductivity of the semiconductor may be impacted by these differences in work function. Higher work function values, as observed in the layers of USP TiO₂, for example, indicate a stronger inclination toward n-type conductivity. Observations has been made that this property promotes faster electron release to the interface and speeds up the development of p-n junctions. These characteristics have consequences for solar cell performance (SC). Improved SC output metrics like Fill Factor (FF) and Voc are correlated with higher work function values. Moreover, the higher work function in USP TiO₂ indicates improved dielectric characteristics. This ultimately results in increased shunt resistance and more successful charge carrier recombination suppression at the interface, both of which are essential for solar cells to operate efficiently.

SUMMARY

Recently, the demand for sustainable, fossil free energy sources has become one of the most challenging topics among the researchers worldwide. Photovoltaic (PV) energy conversion technology is the leading renewable energy resource toward a more sustainable future. The building integrated photovoltaic (BIPV) technology, where solar cells are directly integrated into building elements, such as roofs, windows or roofs is a modern and promising PV technology branch. The semi-transparent solar cells enable simultaneous electricity generation and light transmission.

$\text{Sb}_2(\text{S,Se})_3$ has proven to be a promising photovoltaic material for semi-transparent solar cells due to its' tunable bandgap, high absorption coefficient and nontoxic and earth-abundant constituents. However, material selection, fabrication, and device structure design, are standing challenges remaining to be addressed to improve the performance. One of the core components of solar cell structure is electron transport material which is primary responsible for achieving high-performance solar cells: it promotes the collection of photogenerated electrons from the absorber layer to the bottom electrode as well as suppresses charge carries recombination. Therefore, the properties and the thickness of ETL material, which largely depends on synthesis method and preparation technology is of highest importance.

The objective of this study was to manufacture and study the semitransparent solar cell core component, TiO_2 , electron transport layer and estimate its suitability for the semi transparent solar cell with FTO/ TiO_2 / Sb_2S_3 /P3HT/Au structure. Two reliable synthesis techniques have been chosen to grow TiO_2 – Atom Layer Deposition (ALD) and Ultrasonic Spray Pyrolysis (USP). This study demonstrates that the introduction of a electron conducting layer, TiO_2 into the semi-transparent solar cell device structure is an important step in solar cell technology in order to suppress charge carries recombination and to improve overall efficiency of the device. Both methods chosen for this study for TiO_2 ETL preparation, ALD and USP are reliable, robust and powerful techniques allowing to grow highly reproducible, uniform, pinhole-free TiO_2 thin films with excellent thickness accuracy and conformity at low temperatures. Independent of the growth method, TiO_2 belong to anatase, crystalline TiO_2 phase. However, USP TiO_2 has shown benefits over ALD TiO_2 in terms of better band alignment of SC structure. The CBM band position of USP TiO_2 is 0,39 eV closer to CBM of an Sb_2S_3 absorber compared to CBM of ALD TiO_2 , resulting in a more efficient photogenerated charge-carries separation and more efficient recombination rate suppression. As a result, SC output parameters are somewhat 15% above that those of ALD TiO_2 record sample. The average values of J_{sc} are 14 mA, FF-40% and Eff. 3,5 % of USP TiO_2 SC vs. 12 mA, 35% and 3,0 %, for a record ALD TiO_2 SC, respectively. The performance of SC based on ALD TiO_2 ETL largely depends on a thickness of the later. Too thin

layer, 100 deposition cycles or 5 nm thick layer, is obviously not enough to suppress recombination of carriers and be an efficient transport material. The optimal ALD TiO₂ thickness, resulting in highest output parameters corresponds to 400 ALD deposition cycles or 30 nm, resulting in the highest SC performance (max. eff. Ca. 3.3 %). Thicker ALD TiO₂ films, starting from 800 cycles and above with thicknesses larger than 60 nm have reduced shunt resistance, fill factor and short circuit current values, therefore cutting off the solar cell efficiencies down to 2-2.5%.

For semitransparent solar cell, where other components are synthesized by spray method as well, the USP method is obviously beneficial as it is cheaper, faster and can be produced sequentially on same deposition apparatus prior Sb₂S₃ absorber layer spraying process.

KOKKUVÕTE

Viimasel ajal on nõudlus jätkusuutlike energiaallikate järele muutunud üheks kõige aktuaalsemaks probleemiks teadlaste seas üle maailma. Päikesekiirgust fotoelektrilise muundamise teel elektriks muundav tehnoloogia, fotovolttehnoloogia, on juhtiv taastuvenergia haru säästvama tuleviku suunas. Ehitisintegreeritud päikesepaneelide tehnoloogia, kus päikesepatareid on otseselt integreeritud ehituselementidesse, nagu katused, aknad või seinad, on kaasaegne ja paljutootav päikesetehnoloogia osa.

Poolläbipaistvad päikesepatareid, suurem osa ehitisintegreeritud päikesetehnoloogiast, üheaegselt võimaldavad nii elektrit toota ja kui ka edastada valgust. $Sb_2(S,Se)_3$ on kujunenud uueks atraktiivseks poolläbipaistvaks fotovoltmaterjaliks oma kõrge neeldumisteguri, sobiliku keelutsoonilaiuse ning mittetoksilisuse ja laialdaselt levinud koostisosade poolest. Poolläbipaistvate päikesepatareide jõudluse suurendamiseks on siiski veel palju väljakutseid ees, sealhulgas õige materjali valik, materjalide kokku sobitamine, päikesepaneelide koostisosade valmistamisprotsess, ja seadme struktuuri disain.

Päikesepatareide struktuuri üks põhikomponentidest on elektrontranspordimaterjal, mis vastutab peamiselt suure kasuteguriga päikesepatareide saavutamise eest: see soodustab fotogenereeritud elektronide kogumist absorberikihist alumisse elektroodi ning pärsib laengukandjate rekombinatsiooni. Seetõttu on kõige olulisemad on elektronmaterjali omadused ja paksus, mis sõltuvad suuresti sünteesimeetodist ja valmistamistehnoloogiast.

Antud uuringu eesmärk oli toota ja uurida poolläbipaistvat päikesepatarei põhikomponenti, TiO_2 , elektrontransportkihti ja hinnata selle sobivust FTO/ TiO_2 / Sb_2S_3 /P3HT/Au struktuuriga poolläbipaistvale päikesepatareile. TiO_2 kasvatamiseks on valitud kaks usaldusväärset sünteesimeetodit – aatomikihi sadestamine (ALD) ja ultraheli pihustuspürolüüs (USP). Teostatud uuring näitab, et elektronjuhtiva kihi, TiO_2 , inkorporeerumine poolläbipaistvasse päikesepatareide seadme struktuuri on oluline samm päikesepatareide tehnoloogias, et maha suruda laengukandjate rekombinatsiooni ja tõsta seadme kasutegurit.

Mõlemad TiO_2 ETL ettevalmistamiseks valitud meetodid, ALD ja USP on usaldusväärsed, töökindlad ja võimsad tehnikad, mis võimaldavad kasvatada väga reprodutseeritavaid, ühtlasi, augudeta TiO_2 õhukesi kilesid madalatel temperatuuridel. Sõltumata kasvumeetodist kuuluvad saadud TiO_2 kihid anataasi, kristalsesse TiO_2 faasi. Kuid USP TiO_2 on näidanud eeliseid ALD TiO_2 ees SC struktuuri elektronkonfiguratsiooni positsiooni osas. USP TiO_2 CBM-riba asend on 0,39 eV lähemal Sb_2S_3 absorberi CBM-ile võrreldes ALD TiO_2 CBM-iga, mille tulemuseks on tõhusam fotogenereeritud laengute eraldamine ja tõhusam rekombinatsioonikiiruse surumine. Selle tulemusena on SC väljundparameetrid mõnevõrra 15% kõrgemad kui ALD TiO_2 kõrgeima kasuteguriga päikeseelemendil. J_{sc} keskmised väärtused on vastavalt 14 mA, FF-40% ja Eff. 3,5 % USP TiO_2 SC vs. 12 mA, 35% ja 3,0 %, rekordilise kasuteguriga ALD TiO_2 SC puhul.

ALD TiO₂ ETL-il põhineva SC kasutegur sõltub suuresti selle paksusest. Liiga õhuke kiht, 100 sadestustsükli või 5 nm paksune kiht ei ole küllaldaselt piisav, et pärssida kandjate rekombinatsiooni ja olla tõhus transpordimaterjal. Optimaalne ALD TiO₂ paksus, mille tulemuseks on kõrgeimad väljundparameetrid, vastab 400 ALD sadestustsükli või 30 nm-le, mille tulemuseks on kõrgeim SC kasutegur, 3.3 %.

Paksemad ALD TiO₂ kiled, mis algavad 800 tsüklist ja üle selle paksusega (üle 60 nm), on vähendanud šunditakistust, täitetegurit ja lühisvoolu väärtusi, vähendades seega päikesepatareide kasuteguri 2-2,5% -ni.

Poolläbipaistva päikesepatareide puhul, kus pihustus pürolüüsimeetodiga sünteesitakse ka muid komponente, on USP-meetod ilmselgelt atraktiivsem, kuna see on odavam, kiirem ja päikeseelementi saab toota järjestikku samal sadestusseadmel.

LIST OF REFERENCES

- [1] "Shining brightly | MIT News | Massachusetts Institute of Technology." Accessed: Jul. 05, 2023. [Online]. Available: <https://news.mit.edu/2011/energy-scale-part3-1026>
- [2] "SOLAR ENERGY: POTENTIAL FOR MITIGATING DEVASTATING EFFECTS OF CLIMATE CHANGE | Afribary." Accessed: Jul. 05, 2023. [Online]. Available: <https://afribary.com/works/solar-energy-potential-for-mitigating-devastating-effects-of-climate-change-3599>
- [3] "Perovskite: Solar energy for you and me? | Special-reports – Gulf News." Accessed: Jul. 05, 2023. [Online]. Available: <https://gulfnews.com/special-reports/perovskite-solar-energy-for-you-and-me-1.1680067920437>
- [4] D. Lincot, "The new paradigm of photovoltaics: From powering satellites to powering humanity," *C R Phys*, vol. 18, no. 7–8, pp. 381–390, Sep. 2017, doi: 10.1016/J.CRHY.2017.09.003.
- [5] A.-E. Becquerel, "Recherches sur les effets de la radiation chimique de la lumiere solaire au moyen des courants electriques," *CR Acad. Sci*, vol. 9, no. 145, p. 1, 1839.
- [6] M. E. Becquerel, "Mémoire sur les effets électriques produits sous l'influence des rayons solaires," *C R Hebd Seances Acad Sci*, vol. 9, pp. 561–567, 1839.
- [7] T. Zhang and H. Yang, "High Efficiency Plants and Building Integrated Renewable Energy Systems," *Handbook of Energy Efficiency in Buildings: A Life Cycle Approach*, pp. 441–595, Jan. 2019, doi: 10.1016/B978-0-12-812817-6.00040-1.
- [8] J. A. Nelson, *The physics of solar cells*. World Scientific Publishing Company, 2003.
- [9] M. A. Farhana, A. Manjeevan, and J. Bandara, "Recent advances and new research trends in Sb₂S₃ thin film based solar cells," *Journal of Science: Advanced Materials and Devices*, vol. 8, no. 1, p. 100533, Mar. 2023, doi: 10.1016/j.jsamd.2023.100533.
- [10] C.-Y. Tsai and C.-Y. Tsai, "Tandem amorphous/microcrystalline silicon thin-film solar modules: Developments of novel technologies," *Solar Energy*, vol. 170, pp. 419–429, Aug. 2018, doi: 10.1016/j.solener.2018.05.060.
- [11] Y. Olzhabay, M. N. Hamidi, A. Marzuki, D. Ishak, A. Ng, and I. A. Ukaegbu, "Estimation of Energy Generation from BIPV Samples Based on Perovskite Solar cells in Kazakhstan," in *2022 IEEE International Conference on Power and Energy (PECon)*, IEEE, Dec. 2022, pp. 342–345. doi: 10.1109/PECon54459.2022.9988845.
- [12] S. Shi and N. Zhu, "Challenges and Optimization of Building-Integrated Photovoltaics (BIPV) Windows: A Review," *Sustainability*, vol. 15, no. 22, p. 15876, Nov. 2023, doi: 10.3390/su152215876.
- [13] A. Ruiz-Perona *et al.*, "Semitransparent Wide Bandgap Cu₂ZnGe(S,Se)₄ Thin-Film Solar Cells: Role of the Sulfurization Process," *Solar RRL*, Jan. 2024, doi: 10.1002/solr.202300947.
- [14] Z. Duan *et al.*, "Sb₂Se₃ Thin-Film Solar Cells Exceeding 10% Power Conversion Efficiency Enabled by Injection Vapor Deposition Technology," *Advanced Materials*, vol. 34, no. 30, Jul. 2022, doi: 10.1002/adma.202202969.
- [15] S. Barthwal, S. Singh, A. K. Chauhan, N. S. Prabhu, A. G. Prabhudessai, and K. Ramesh, "A comprehensive insight into deep-level defect engineering in antimony chalcogenide solar cells," *Mater Adv*, vol. 4, no. 23, pp. 5998–6030, 2023, doi: 10.1039/D3MA00479A.
- [16] A. Alexandrov, M. Zvaigzne, D. Lypenko, I. Nabiev, and P. Samokhvalov, "Al-, Ga-, Mg-, or Li-doped zinc oxide nanoparticles as electron transport layers for quantum dot light-emitting diodes," *Sci Rep*, vol. 10, no. 1, p. 7496, May 2020, doi: 10.1038/s41598-020-64263-2.
- [17] Y. Dou *et al.*, "High-Efficiency Layer-by-Layer All-Polymer Solar Cell Enabled by Bottom-Layer Optimization," *Solar RRL*, vol. 7, no. 22, Nov. 2023, doi: 10.1002/solr.202300599.
- [18] S. Zheng, G. Wang, T. Liu, L. Lou, S. Xiao, and S. Yang, "Materials and structures for the electron transport layer of efficient and stable perovskite solar cells," *Sci China*

- Chem*, vol. 62, no. 7, pp. 800–809, Jul. 2019, doi: 10.1007/s11426-019-9469-1.
- [19] G. Zaiats, S. Ikeda, and P. V. Kamat, "Optimization of the electron transport layer in quantum dot light-emitting devices," *NPG Asia Mater*, vol. 12, no. 1, p. 57, Dec. 2020, doi: 10.1038/s41427-020-00237-0.
- [20] E. Kärber, A. Katerski, I. Oja Acik, A. Mere, V. Mikli, and M. Krunks, "Sb₂S₃ grown by ultrasonic spray pyrolysis and its application in a hybrid solar cell," *Beilstein Journal of Nanotechnology*, vol. 7, pp. 1662–1673, Nov. 2016, doi: 10.3762/bjnano.7.158.
- [21] J. S. Eensalu, A. Katerski, E. Kärber, I. Oja Acik, A. Mere, and M. Krunks, "Uniform Sb₂S₃ optical coatings by chemical spray method," *Beilstein Journal of Nanotechnology*, vol. 10, pp. 198–210, Jan. 2019, doi: 10.3762/bjnano.10.18.
- [22] M. Tabakovic *et al.*, "Status and Outlook for Building Integrated Photovoltaics (BIPV) in Relation to Educational needs in the BIPV Sector," *Energy Procedia*, vol. 111, pp. 993–999, Mar. 2017, doi: 10.1016/J.EGYPRO.2017.03.262.
- [23] "EUR-Lex - 32010L0031 - EN - EUR-Lex." Accessed: Feb. 07, 2023. [Online]. Available: https://eur-lex.europa.eu/legal-content/EN/ALL/;ELX_SESSIONID=FZMjThLLzfxmmMCQGp2Y1s2d3Tjwtd8QS3pqdkhXZbwqGwlgY9KN!2064651424?uri=CELEX:32010L0031
- [24] "EUR-Lex - 32012L0027 - EN - EUR-Lex." Accessed: Feb. 07, 2023. [Online]. Available: <https://eur-lex.europa.eu/legal-content/EN/TXT/?qid=1399375464230&uri=CELEX:32012L0027>
- [25] G. Happle, Z. Shi, S. Hsieh, B. Ong, J. A. Fonseca, and A. Schlueter, "Identifying carbon emission reduction potentials of BIPV in high-density cities in Southeast Asia," *J Phys Conf Ser*, vol. 1343, no. 1, p. 012077, Nov. 2019, doi: 10.1088/1742-6596/1343/1/012077.
- [26] M. Tian, R. Tao, L. Dong, and H. Li, "BIPV Generation Efficiency Optimal Scheme—Take Jiangning District of Nanjing City for Example," *Highlights in Science, Engineering and Technology*, vol. 64, pp. 1–16, Aug. 2023, doi: 10.54097/hset.v64i.11238.
- [27] C. Wen, Y. Zhang, and Y. Zhao, "Application of phase change materials in photovoltaic building integration system," in *2022 International Conference on Optoelectronic Information and Functional Materials (OIFM 2022)*, C. Zuo, Ed., SPIE, Apr. 2022, p. 66. doi: 10.1117/12.2639059.
- [28] R. Juškėnas, A. Naujokaitis, A. Drabavičius, V. Pakštas, D. Vainauskas, and R. Kondrotas, "Seed Layer Optimisation for Ultra-Thin Sb₂Se₃ Solar Cells on TiO₂ by Vapour Transport Deposition," *Materials*, vol. 15, no. 23, p. 8356, Nov. 2022, doi: 10.3390/ma15238356.
- [29] M. K. Hossain *et al.*, "An extensive study on multiple ETL and HTL layers to design and simulation of high-performance lead-free CsSnCl₃-based perovskite solar cells," *Sci Rep*, vol. 13, no. 1, p. 2521, Feb. 2023, doi: 10.1038/s41598-023-28506-2.
- [30] P. Kumar, S. You, and A. Vomiero, "CuSCN as a hole transport layer in an inorganic solution-processed planar Sb₂S₃ solar cell, enabling carbon-based and semitransparent photovoltaics," *J Mater Chem C Mater*, vol. 10, no. 43, pp. 16273–16282, 2022, doi: 10.1039/D2TC03420D.
- [31] L. J. Foruzin, Z. Rezvani, and K. Nejati, "Fabrication of TiO₂@ZnAl-layered double hydroxide based anode material for dye-sensitized solar cell," *RSC Adv*, vol. 6, no. 13, pp. 10912–10918, 2016, doi: 10.1039/C5RA23384D.
- [32] C. D. Weber, D. P. Stay, and M. C. Lonergan, "Effects of Polyfluorene Polyelectrolyte Interfacial Layers on Selectivity and Recombination Measured Using the Interdigitated Back-Contact Solar Cell," *The Journal of Physical Chemistry C*, vol. 120, no. 36, pp. 19951–19960, Sep. 2016, doi: 10.1021/acs.jpcc.6b03783.
- [33] L. Lin *et al.*, "Inorganic Electron Transport Materials in Perovskite Solar Cells," *Adv Funct Mater*, vol. 31, no. 5, Jan. 2021, doi: 10.1002/adfm.202008300.
- [34] J. Hai *et al.*, "Dopant-Free Hole Transport Materials Based on a Large Conjugated Electron-Deficient Core for Efficient Perovskite Solar Cells," *Adv Funct Mater*, vol. 31, no. 51, Dec. 2021, doi: 10.1002/adfm.202105458.
- [35] A. A. Said, J. Xie, and Q. Zhang, "Recent Progress in Organic Electron Transport Materials in Inverted Perovskite Solar Cells," *Small*, vol. 15, no. 27, Jul. 2019, doi:

- 10.1002/sml.201900854.
- [36] K. Valadi, S. Gharibi, R. Taheri-Ledari, S. Akin, A. Maleki, and A. E. Shalan, "Metal oxide electron transport materials for perovskite solar cells: a review," *Environ Chem Lett*, vol. 19, no. 3, pp. 2185–2207, Jun. 2021, doi: 10.1007/s10311-020-01171-x.
- [37] Y. C. Choi, D. U. Lee, J. H. Noh, E. K. Kim, and S. Il Seok, "Highly Improved Sb₂S₃ Sensitized-Inorganic–Organic Heterojunction Solar Cells and Quantification of Traps by Deep-Level Transient Spectroscopy," *Adv Funct Mater*, vol. 24, no. 23, pp. 3587–3592, Jun. 2014, doi: 10.1002/ADFM.201304238.
- [38] M. Dkhili *et al.*, "Attributes of High-Performance Electron Transport Layers for Perovskite Solar Cells on Flexible PET versus on Glass," *ACS Appl Energy Mater*, vol. 5, no. 4, pp. 4096–4107, Apr. 2022, doi: 10.1021/acsaem.1c03311.
- [39] P. Subudhi and D. Punetha, "Pivotal avenue for hybrid electron transport layer-based perovskite solar cells with improved efficiency," *Sci Rep*, vol. 13, no. 1, p. 19485, Nov. 2023, doi: 10.1038/s41598-023-33419-1.
- [40] C. Ou, K. Shen, Z. Li, H. Zhu, T. Huang, and Y. Mai, "Bandgap tunable CdS:O as efficient electron buffer layer for high-performance Sb₂Se₃ thin film solar cells," *Solar Energy Materials and Solar Cells*, vol. 194, pp. 47–53, Jun. 2019, doi: 10.1016/j.solmat.2019.01.043.
- [41] J. Zhou *et al.*, "Colloidal SnO₂-Assisted CdS Electron Transport Layer Enables Efficient Electron Extraction for Planar Perovskite Solar Cells," *Solar RRL*, vol. 5, no. 9, Sep. 2021, doi: 10.1002/solr.202100494.
- [42] D. Mardare, M. Tasca, M. Delibas, and G. I. Rusu, "On the structural properties and optical transmittance of TiO₂ r.f. sputtered thin films," *Appl Surf Sci*, vol. 156, no. 1–4, pp. 200–206, Feb. 2000, doi: 10.1016/S0169-4332(99)00508-5.
- [43] M. Hadi. Shinen, S. A. A. AlSaati, and F. Z. Razooqi, "Preparation of high transmittance TiO₂ thin films by sol-gel technique as antireflection coating," *J Phys Conf Ser*, vol. 1032, p. 012018, May 2018, doi: 10.1088/1742-6596/1032/1/012018.
- [44] J.-P. Niemelä, G. Marin, and M. Karppinen, "Titanium dioxide thin films by atomic layer deposition: a review," *Semicond Sci Technol*, vol. 32, no. 9, p. 093005, Sep. 2017, doi: 10.1088/1361-6641/aa78ce.
- [45] S. T. Barry, "Chemistry of Atomic Layer Deposition," *Chemistry of Atomic Layer Deposition*, Nov. 2021, doi: 10.1515/9783110712537/HTML.
- [46] J. Bachmann *et al.*, "Size effects in ordered arrays of magnetic nanotubes: Pick your reversal mode," *J Appl Phys*, vol. 105, no. 7, 2009, doi: 10.1063/1.3074109.
- [47] S. M. George, "Atomic layer deposition: An overview," *Chem Rev*, vol. 110, no. 1, pp. 111–131, Jan. 2010, doi: 10.1021/CR900056B.
- [48] M. Knez, K. Nielsch, and L. Niinistö, "Synthesis and surface engineering of complex nanostructures by atomic layer deposition," *Advanced Materials*, vol. 19, no. 21, pp. 3425–3438, Nov. 2007, doi: 10.1002/ADMA.200700079.
- [49] T. P. Brennan *et al.*, "Atomic layer deposition of CDS quantum dots for solid-state quantum dot sensitized solar cells," *Adv Energy Mater*, vol. 1, no. 6, pp. 1169–1175, Nov. 2011, doi: 10.1002/AENM.201100363.
- [50] R. Kondrotas, C. Chen, and J. Tang, "Sb₂S₃ Solar Cells," *Joule*, vol. 2, no. 5, pp. 857–878, May 2018, doi: 10.1016/J.JOULE.2018.04.003.
- [51] X. Wang, R. Tang, C. Wu, C. Zhu, and T. Chen, "Development of antimony sulfide–selenide Sb₂(S, Se)₃-based solar cells," *Journal of Energy Chemistry*, vol. 27, no. 3, pp. 713–721, May 2018, doi: 10.1016/J.JECHEM.2017.09.031.
- [52] S. T. Barry, "Chemistry of Atomic Layer Deposition," *Chemistry of Atomic Layer Deposition*, Jul. 2021, doi: 10.1515/9783110712537/HTML.
- [53] I. Kupa *et al.*, "Optical, Electrical, and Crystal Properties of TiO₂ Thin Films Grown by Atomic Layer Deposition on Silicon and Glass Substrates," vol. 47, doi: 10.1007/s11664-018-6370-y.
- [54] J. Aarik, A. Aidla, H. Mändar, and T. Uustare, "Atomic layer deposition of titanium dioxide from TiCl₄ and H₂O: investigation of growth mechanism," *Appl Surf Sci*, vol. 172, no. 1–2, pp. 148–158, Mar. 2001, doi: 10.1016/S0169-4332(00)00842-4.
- [55] M. Shahmohammadi, R. Mukherjee, C. Sukotjo, U. Diwekar, and C. Takoudis, "Recent

- Advances in Theoretical Development of Thermal Atomic Layer Deposition: A Review," *Nanomaterials*, vol. 12, no. 5, p. 831, Mar. 2022, doi: 10.3390/nano12050831.
- [56] B. C. Mallick, C.-T. Hsieh, K.-M. Yin, Y. A. Gandomi, and K.-T. Huang, "Review—On Atomic Layer Deposition: Current Progress and Future Challenges," *ECS Journal of Solid State Science and Technology*, vol. 8, no. 4, pp. N55–N78, May 2019, doi: 10.1149/2.0201903jss.
- [57] J. Yim, E. Verkama, J. A. Velasco, K. Arts, and R. L. Puurunen, "Conformality of atomic layer deposition in microchannels: impact of process parameters on the simulated thickness profile," *Physical Chemistry Chemical Physics*, vol. 24, no. 15, pp. 8645–8660, 2022, doi: 10.1039/D1CP04758B.
- [58] Y. Zhang *et al.*, "Atomic Layer Deposition of Titanium Oxide on Single-Layer Graphene: An Atomic-Scale Study toward Understanding Nucleation and Growth," *Chemistry of Materials*, vol. 29, no. 5, pp. 2232–2238, Mar. 2017, doi: 10.1021/acs.chemmater.6b05143.
- [59] S. W. Kim, D. Y. Kim, H. H. Roh, H. S. Kim, J. W. Lee, and K. Y. Lee, "Three-Dimensional Bioprinting of Cell-Laden Constructs Using Polysaccharide-Based Self-Healing Hydrogels," *Biomacromolecules*, vol. 20, no. 5, pp. 1860–1866, May 2019, doi: 10.1021/acs.biomac.8b01589.
- [60] S. Rahemi Ardekani, A. Sabour Rouh Aghdam, M. Nazari, A. Bayat, E. Yazdani, and E. Saievar-Iranizad, "A comprehensive review on ultrasonic spray pyrolysis technique: Mechanism, main parameters and applications in condensed matter," *J Anal Appl Pyrolysis*, vol. 141, p. 104631, Aug. 2019, doi: 10.1016/j.jaap.2019.104631.
- [61] P. Majerič and R. Rudolf, "Advances in Ultrasonic Spray Pyrolysis Processing of Noble Metal Nanoparticles—Review," *Materials*, vol. 13, no. 16, p. 3485, Aug. 2020, doi: 10.3390/ma13163485.
- [62] J. S. Eensalu, M. Krunks, I. Gromyko, A. Katerski, and A. Mere, "A comparative study on physical properties of Al-doped zinc oxide thin films deposited from zinc acetate and zinc acetylacetonate by spray pyrolysis," *Energetika*, vol. 63, no. 2, Sep. 2017, doi: 10.6001/energetika.v63i2.3519.
- [63] J. S. Eensalu, A. Katerski, E. Kärber, I. Oja Acik, A. Mere, and M. Krunks, "Uniform Sb₂S₃ optical coatings by chemical spray method," *Beilstein Journal of Nanotechnology*, vol. 10, pp. 198–210, Jan. 2019, doi: 10.3762/bjnano.10.18.
- [64] W. Naffouti, A. Jrad, T. Ben Nasr, S. Ammar, and N. Turki-Kamoun, "Structural, morphological and optical properties of TiO₂:Mn thin films prepared by spray pyrolysis technique," *Journal of Materials Science: Materials in Electronics*, vol. 27, no. 5, pp. 4622–4630, May 2016, doi: 10.1007/s10854-016-4339-2.
- [65] D. Golub, A. Ivanič, P. Majerič, H. R. Tiyyagura, I. Anžel, and R. Rudolf, "Synthesis of Colloidal Au Nanoparticles through Ultrasonic Spray Pyrolysis and Their Use in the Preparation of Polyacrylate-AuNPs' Composites," *Materials*, vol. 12, no. 22, p. 3775, Nov. 2019, doi: 10.3390/ma12223775.
- [66] Z. Chen, I. Dündar, I. Oja Acik, and A. Mere, "TiO₂ thin films by ultrasonic spray pyrolysis," *IOP Conf Ser Mater Sci Eng*, vol. 503, p. 012006, Mar. 2019, doi: 10.1088/1757-899X/503/1/012006.
- [67] "Ultrasonic Spray Pyrolysis." Accessed: Dec. 03, 2023. [Online]. Available: <https://www.hielscher.com/ultrasonic-spray-pyrolysis.htm>
- [68] M. T. Taschuk, M. M. Hawkeye, and M. J. Brett, "Glancing Angle Deposition," in *Handbook of Deposition Technologies for Films and Coatings*, Elsevier, 2010, pp. 621–678. doi: 10.1016/B978-0-8155-2031-3.00013-2.
- [69] R. Suresh, V. Ponnuswamy, and R. Mariappan, "Effect of solvent and substrate temperature on morphology of cerium oxide thin films by simple nebuliser spray pyrolysis technique," *Materials Technology*, vol. 30, no. 1, pp. 12–22, Jan. 2015, doi: 10.1179/1753555714Y.0000000183.
- [70] R. Taziwa and E. Meyer, "Fabrication of TiO₂ Nanoparticles and Thin Films by Ultrasonic Spray Pyrolysis: Design and Optimization," in *Pyrolysis*, InTech, 2017. doi: 10.5772/67866.
- [71] L. Mino, C. Negri, R. Santalucia, G. Cerrato, G. Spoto, and G. Martra, "Morphology,

- Surface Structure and Water Adsorption Properties of TiO₂ Nanoparticles: A Comparison of Different Commercial Samples," *Molecules*, vol. 25, no. 20, p. 4605, Oct. 2020, doi: 10.3390/molecules25204605.
- [72] F. Zeribi *et al.*, "Dependence of the Physical Properties of Titanium Dioxide (TiO₂) Thin Films Grown by Sol-Gel (Spin-Coating) Process on Thickness," *ECS Journal of Solid State Science and Technology*, vol. 11, no. 2, p. 023003, Feb. 2022, doi: 10.1149/2162-8777/ac5168.
- [73] A. Taherniya and D. Raoufi, "Thickness dependence of structural, optical and morphological properties of sol-gel derived TiO₂ thin film," *Mater Res Express*, vol. 6, no. 1, p. 016417, Oct. 2018, doi: 10.1088/2053-1591/aae4d0.
- [74] R. Singh, M. Gupta, D. M. Phase, and S. K. Mukherjee, "Phase growth analysis of sputtered TiO₂ thin films at low oxygen partial pressures using XANES and XRR," *Mater Res Express*, vol. 6, no. 11, p. 116449, Oct. 2019, doi: 10.1088/2053-1591/ab4e3f.
- [75] A. S. Rini, M. P. Deraf, Y. Hamzah, and A. A. Umar, "Optical, structural and morphological studies of TiO₂ thin film synthesized by liquid phase deposition method," 2020, p. 080015. doi: 10.1063/5.0003175.
- [76] M. Ben Karoui, Z. Kaddachi, and R. Gharbi, "Optical properties of nanostructured TiO₂ thin films," *J Phys Conf Ser*, vol. 596, p. 012012, Apr. 2015, doi: 10.1088/1742-6596/596/1/012012.
- [77] M. H. Mithun, A. Sayed, and I. Rahaman, "The Effect of Band-Gap on TiO₂ Thin Film Considering Various Parameters," *Proceedings of Engineering and Technology Innovation*, vol. 19, pp. 45–52, Jul. 2021, doi: 10.46604/peti.2021.7712.
- [78] O. Durante *et al.*, "Emergence and Evolution of Crystallization in TiO₂ Thin Films: A Structural and Morphological Study," *Nanomaterials*, vol. 11, no. 6, p. 1409, May 2021, doi: 10.3390/nano11061409.
- [79] S. Kashiwaya, J. Morasch, V. Streibel, T. Toupance, W. Jaegermann, and A. Klein, "The Work Function of TiO₂," *Surfaces*, vol. 1, no. 1, pp. 73–89, Sep. 2018, doi: 10.3390/surfaces1010007.
- [80] O. Ben khetta *et al.*, "Precursor concentration effect on the physical properties of transparent titania (Anatase-TiO₂) thin films grown by ultrasonic spray process for optoelectronics application," *Opt Mater (Amst)*, vol. 132, p. 112790, Oct. 2022, doi: 10.1016/j.optmat.2022.112790.
- [81] A. Arunachalam, S. Dhanapandian, C. Manoharan, and R. Sridhar, "Characterization of sprayed TiO₂ on ITO substrates for solar cell applications," *Spectrochim Acta A Mol Biomol Spectrosc*, vol. 149, pp. 904–912, Oct. 2015, doi: 10.1016/j.saa.2015.05.014.
- [82] F. López de la Rosa, R. Sánchez-Reolid, J. L. Gómez-Sirvent, R. Morales, and A. Fernández-Caballero, "A Review on Machine and Deep Learning for Semiconductor Defect Classification in Scanning Electron Microscope Images," *Applied Sciences*, vol. 11, no. 20, p. 9508, Oct. 2021, doi: 10.3390/app11209508.
- [83] Y. Yan, "Tribology and tribo-corrosion testing and analysis of metallic biomaterials," in *Metals for Biomedical Devices*, Elsevier, 2010, pp. 178–201. doi: 10.1533/9781845699246.2.178.
- [84] Y. Alqaheem and A. A. Alomair, "Microscopy and Spectroscopy Techniques for Characterization of Polymeric Membranes," *Membranes (Basel)*, vol. 10, no. 2, p. 33, Feb. 2020, doi: 10.3390/membranes10020033.
- [85] B. Dery and L. Zaixiang, "Scanning Electron Microscopy (SEM) as an Effective Tool for Determining the Morphology and Mechanism of Action of Functional Ingredients," *Food Reviews International*, vol. 39, no. 4, pp. 2007–2026, May 2023, doi: 10.1080/87559129.2021.1939368.
- [86] A. Ul-Hamid, "Components of the SEM," in *A Beginners' Guide to Scanning Electron Microscopy*, Cham: Springer International Publishing, 2018, pp. 15–76. doi: 10.1007/978-3-319-98482-7_2.
- [87] Robert Krautmann, Nicolae SpalatuI, and Ilona Oja Açık, "ETIS." Accessed: Jul. 02, 2023. [Online]. Available: <https://www.etis.ee/Portal/Mentorships/Display/b230c9e4-f108-49c4-b980-af9de559c633?lang=ENG>
- [88] Edinst, "UV Vis Spectroscopy | Spectrometer | Spectroscopy Applications." Accessed:

- Jul. 02, 2023. [Online]. Available: <https://www.edinst.com/techniques/uv-vis-spectroscopy/>
- [89] afsin Kariper, E. Güneri, F. Göde, and C. Gümüş, "Effect of pH on the physical properties of CdS thin films deposited by CBD," *Chalcogenide Letters*, vol. 9, pp. 27–40, Jul. 2012.
- [90] R. Kohli and K. L. Mittal, *Developments in surface contamination and cleaning, volume 12: Methods for assessment and verification of cleanliness of surfaces and characterization of surface contaminants*. Elsevier, 2019.
- [91] Knovel, "Knovel - Qualitative Analysis- Handbook of Analytical Techniques in Concrete Science and Technology." Accessed: Jul. 02, 2023. [Online]. Available: <https://app.knovel.com/web/view/khtml/show.v/rcid:kpHATCST01/cid:kt0052L1C7/vi/?view=collapsed>
- [92] "waves - Minimum distance for two parallel beam to interfere effectively - Physics Stack Exchange." Accessed: Dec. 04, 2023. [Online]. Available: <https://physics.stackexchange.com/questions/669504/minimum-distance-for-two-parallel-beam-to-interfere-effectively>
- [93] P. Würfel, "Physics of Solar Cells: From Principles to New Concepts," *Physics of Solar Cells: From Principles to New Concepts*, pp. 1–186, Jul. 2007, doi: 10.1002/9783527618545.
- [94] R. Krautmann *et al.*, "Low processing temperatures explored in Sb₂S₃ solar cells by close-spaced sublimation and analysis of bulk and interface related defects," *Solar Energy Materials and Solar Cells*, vol. 251, p. 112139, Mar. 2023, doi: 10.1016/j.solmat.2022.112139.
- [95] Antonio Luque and Steven Hegedus, *Handbook of Photovoltaic Science and Engineering*. Wiley, 2010. doi: 10.1002/9780470974704.
- [96] C. Pham, "Functional graphene: synthesis, characterization and application in optoelectronics," 2015.
- [97] H. K. Christenson and N. H. Thomson, "The nature of the air-cleaved mica surface," *Surf Sci Rep*, vol. 71, no. 2, pp. 367–390, Jun. 2016, doi: 10.1016/j.surfrep.2016.03.001.
- [98] V. W. Bergmann *et al.*, "Local Time-Dependent Charging in a Perovskite Solar Cell," *ACS Appl Mater Interfaces*, vol. 8, no. 30, pp. 19402–19409, Aug. 2016, doi: 10.1021/acsami.6b04104.
- [99] T. Schultz *et al.*, "Reliable Work Function Determination of Multicomponent Surfaces and Interfaces: The Role of Electrostatic Potentials in Ultraviolet Photoelectron Spectroscopy," *Adv Mater Interfaces*, vol. 4, no. 19, Oct. 2017, doi: 10.1002/admi.201700324.
- [100] L. Liu and G. Li, "Electrical characterization of single-walled carbon nanotubes in organic solar cells by Kelvin probe force microscopy," *Appl Phys Lett*, vol. 96, no. 8, Feb. 2010, doi: 10.1063/1.3332489.
- [101] S. Sadewasser, Th. Glatzel, R. Shikler, Y. Rosenwaks, and M. Ch. Lux-Steiner, "Resolution of Kelvin probe force microscopy in ultrahigh vacuum: comparison of experiment and simulation," *Appl Surf Sci*, vol. 210, no. 1–2, pp. 32–36, Mar. 2003, doi: 10.1016/S0169-4332(02)01475-7.
- [102] A. Sohn, T. Kanki, K. Sakai, H. Tanaka, and D.-W. Kim, "Fractal Nature of Metallic and Insulating Domain Configurations in a VO₂ Thin Film Revealed by Kelvin Probe Force Microscopy," *Sci Rep*, vol. 5, no. 1, p. 10417, May 2015, doi: 10.1038/srep10417.
- [103] J. R. Harwell *et al.*, "Probing the energy levels of perovskite solar cells via Kelvin probe and UV ambient pressure photoemission spectroscopy," *Physical Chemistry Chemical Physics*, vol. 18, no. 29, pp. 19738–19745, 2016, doi: 10.1039/C6CP02446G.
- [104] J. Egedal, W. Daughton, and A. Le, "Large-scale electron acceleration by parallel electric fields during magnetic reconnection," *Nat Phys*, vol. 8, no. 4, pp. 321–324, Apr. 2012, doi: 10.1038/nphys2249.
- [105] R. G. Buchheit, "Corrosion Resistant Coatings and Paints," in *Handbook of Environmental Degradation of Materials*, Elsevier, 2012, pp. 539–568. doi: 10.1016/B978-1-4377-3455-3.00018-3.
- [106] J. E. Yater, "Secondary electron emission and vacuum electronics," *J Appl Phys*, vol. 133, no. 5, Feb. 2023, doi: 10.1063/5.0130972.

- [107] K. G. Nakamura, "Coherent Control of Optical Phonons in Solids," in *Encyclopedia of Interfacial Chemistry*, Elsevier, 2018, pp. 334–337. doi: 10.1016/B978-0-12-409547-2.13236-6.
- [108] H. Ishii, H. Kinjo, T. Sato, S. Machida, and Y. Nakayama, "Photoelectron Yield Spectroscopy for Organic Materials and Interfaces," 2015, pp. 131–155. doi: 10.1007/978-4-431-55206-2_8.
- [109] H. Ishii, "Photoelectron Yield Spectroscopy," in *Compendium of Surface and Interface Analysis*, Singapore: Springer Singapore, 2018, pp. 457–463. doi: 10.1007/978-981-10-6156-1_75.
- [110] S. Tadano, Y. Nakayama, H. Kinjo, H. Ishii, and P. Krüger, "Obtaining the Highest Occupied Molecular Orbital Peak of Organic Matter from Photoelectron Yield Spectra," *Phys Rev Appl*, vol. 11, no. 5, p. 054081, May 2019, doi: 10.1103/PhysRevApplied.11.054081.
- [111] G. Jeantelot *et al.*, "Morphology control of anatase TiO₂ for well-defined surface chemistry," *Physical Chemistry Chemical Physics*, vol. 20, no. 21, pp. 14362–14373, 2018, doi: 10.1039/C8CP01983E.
- [112] S. Qudisia *et al.*, "Role of Surface Coverage and Film Quality of the TiO₂ Electron Selective Layer for Optimal Hole-Blocking Properties," *ACS Omega*, vol. 7, no. 14, pp. 11688–11695, Apr. 2022, doi: 10.1021/acsomega.1c06622.
- [113] A. V. Almaev, N. N. Yakovlev, D. A. Almaev, M. G. Verkholetov, G. A. Rudakov, and K. I. Litvinova, "High Oxygen Sensitivity of TiO₂ Thin Films Deposited by ALD," *Micromachines (Basel)*, vol. 14, no. 10, p. 1875, Sep. 2023, doi: 10.3390/mi14101875.
- [114] M. Hannula, H. Ali-Löytty, K. Lahtonen, E. Sarlin, J. Saari, and M. Valden, "Improved Stability of Atomic Layer Deposited Amorphous TiO₂ Photoelectrode Coatings by Thermally Induced Oxygen Defects," *Chemistry of Materials*, vol. 30, no. 4, pp. 1199–1208, Feb. 2018, doi: 10.1021/acs.chemmater.7b02938.
- [115] E. Riyanto *et al.*, "The growth mechanisms of TiO₂ film onto PET surfaces by atomic layer deposition," *Mater Res Express*, vol. 10, no. 9, p. 096401, Sep. 2023, doi: 10.1088/2053-1591/acf650.
- [116] L. Wang *et al.*, "Stable 6%-efficient Sb₂Se₃ solar cells with a ZnO buffer layer," *Nat Energy*, vol. 2, no. 4, pp. 1–9, Mar. 2017, doi: 10.1038/NENERGY.2017.46.
- [117] R. Tang *et al.*, "n-Type Doping of Sb₂S₃ Light-Harvesting Films Enabling High-Efficiency Planar Heterojunction Solar Cells," *ACS Appl Mater Interfaces*, vol. 10, no. 36, pp. 30314–30321, Sep. 2018, doi: 10.1021/ACSAMI.8B08965.
- [118] Z. Zhang *et al.*, "DMSO-Free Solvent Strategy for Stable and Efficient Methylammonium-Free Sn–Pb Alloyed Perovskite Solar Cells," *Adv Energy Mater*, vol. 13, no. 17, May 2023, doi: 10.1002/aenm.202300181.
- [119] M. Rusu *et al.*, "Electronic Structure of the CdS/Cu(In,Ga)Se₂ Interface of KF- and RbF-Treated Samples by Kelvin Probe and Photoelectron Yield Spectroscopy," *ACS Appl Mater Interfaces*, vol. 13, no. 6, pp. 7745–7755, Feb. 2021, doi: 10.1021/acsami.0c20976.
- [120] C. Zhou *et al.*, "Unveiling Charge Carrier Recombination, Extraction, and Hot-Carrier Dynamics in Indium Incorporated Highly Efficient and Stable Perovskite Solar Cells," *Advanced Science*, vol. 9, no. 11, Apr. 2022, doi: 10.1002/advs.202103491.

